

Full Length Research Paper

Detection of acute hypotensive episodes via a trained adaptive network-based fuzzy inference system (ANFIS)

A. Ghaffari^{1,2}, M. R. Homaeinezhad^{1,2*}, M. Atarod², M. Akraminia^{1,2} and H. Najjaran Toosi^{1,2}

¹CardioVascular Research Group (CVRG), Iran.

²Department of Mechanical Engineering, K. N. Toosi University of Technology, No. 15, Pardis Street, Mollasadra Avenue, Vanak Sq., Tehran, P. O. Box 19395-1999, Iran.

Accepted 27 September, 2009

The aim of this study is to detect acute hypotensive episodes (AHE) and mean arterial pressure dropping regimes (MAPDRs) using ECG signal and arterial blood pressure (ABP) waveforms. To meet this end, the QRS complexes and end-systolic end-diastolic pulses are first extracted using two innovative modified Hilbert transform-based algorithms namely as ECGMHT and BPMHT. The resulted systolic blood pressure (SBP) and diastolic blood pressure (DBP) pulses are then used to calculate the mean arterial pressure (MAP) trend. A new smoothing algorithm is then developed based on piecewise polynomial fitting (PPF) to smooth the fast fluctuations observed in RR-tachogram and MAP trend. The PPF algorithm operates by sequentially fitting N number of polynomials to the original signal and calculating the corresponding coefficients using the best linear unbiased estimation (BLUE) approach. Afterwards, in order to consider the mutual influence of parameters on the evaluation of shock probability, a Sugeno adaptive network-based fuzzy inference system-ANFIS is trained using Hasdai et al. parameters as input, with appropriate membership functions for each parameter. Using this network, it will be possible to incorporate the possible mutual influences between risk parameters such as heart rate (HR), systolic blood pressure (SBP), diastolic blood pressure (DBP), age, gender, weight and some miscellaneous factors to the calculation of shock occurrence probability. In the next step, the proposed algorithm is applied to 15 subjects of the MIMIC II Database and AHE and MAPDRs (MAP \leq 60 mmHg with a period of 30 min or more) are identified. As a result of this study, MAPDR is realized as a specific marker of cardiogenic shock. In that, for a sequence of MAPDRs; as long as 20 min or more, there will exist a consequent high peak with the duration of 3 to 4 min in the corresponding probability of cardiogenic shock diagram. The presented algorithm did not yield any inappropriate or wrong results on MIMICII database (that is False Negative = False Positive = 0).

Key words: Acute hypotensive episode, cardiogenic shock, blood pressure pulse detection, piecewise polynomial fitting, ANFIS approximation.

INTRODUCTION

AHE is one of the most critical events that occur in intensive care units (ICUs) which requires effective and prompt interventions. It is generally defined as any period of 30 min or more during which at least 90% of the MAP measurements are at or below 60 mmHg (Guyton, 1996). AHE can lead to intense organ damage and death if not treated appropriately. Diagnosing the causes of this episode including sepsis, myocardial infarction, cardiac

arrhythmia, pulmonary embolism, hemorrhage, dehydration, hypovolemia, insufficient cardiac output, or vasodilatory shock and conducting timely and proper interventions can remarkably reduce the risk of this fatal episode (Harrison, 2007; Irwin and Rippe, 2003; Paul, 1978).

In this context, Cowley et al. (1973) investigated the role of the baroreceptor reflex in daily control of arterial blood pressure (ABP) and concluded that the hypotension in denervated dogs was proportional to the preexisting arterial blood pressure level. Hasdai et al. (1999) analyzed baseline variables associated with the development of shock after thrombolytic therapy and devised a

*Corresponding author. E-mail: mrezahomaei@yahoo.com.
Tel: +98-21- 84063381.

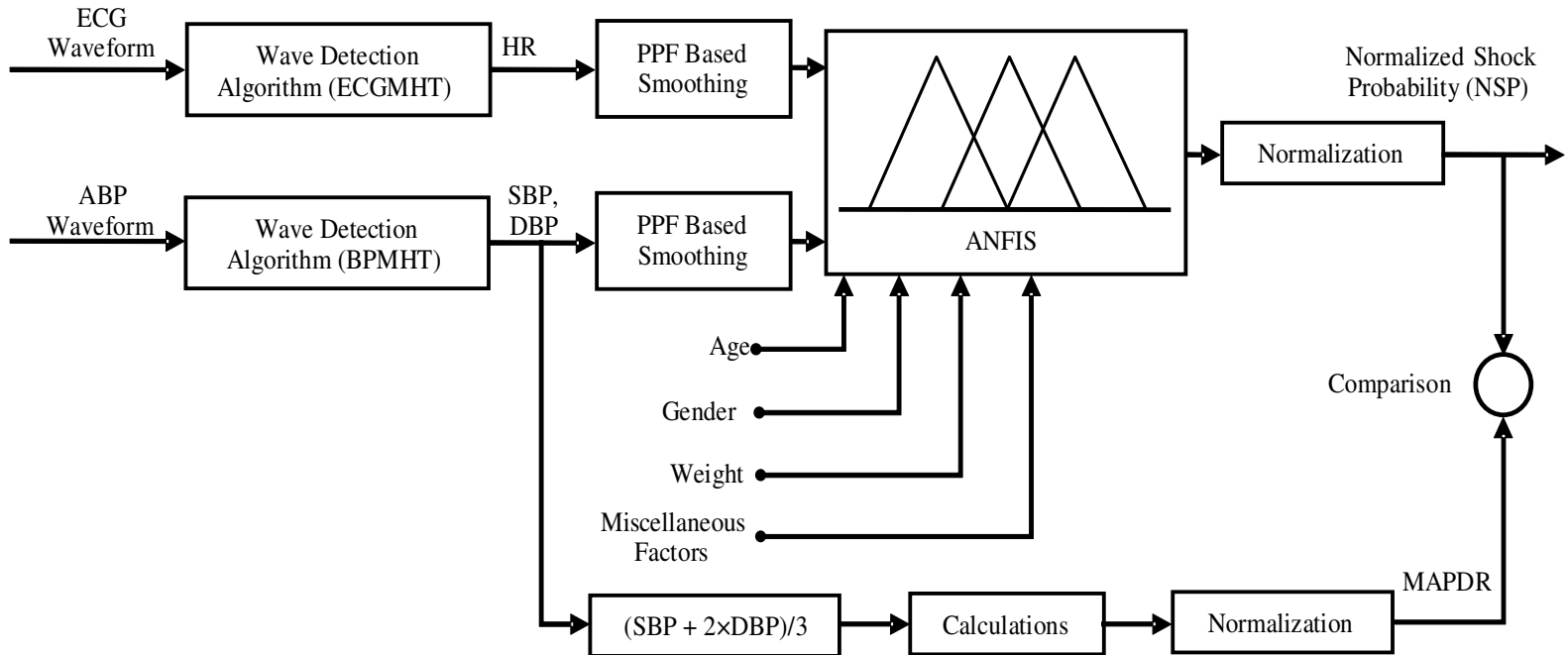


Figure 1. General overview of the proposed shock probability evaluation algorithm via and ANFIS trained model.

scoring system predicting the risk of shock. An innovative study was then conducted by Picard et al. (2002:2003) to identify the echocardiographic features of cardiogenic shock and assess the advantages of findings on early echocardiograms that are associated with mortality after cardiogenic shock. Afterwards, Morris et al. (2002:2005) proposed a potential algorithm for hypotension based on reports of hypotension during anesthesia from the first 4000 incidents reported to the Australian incident monitoring study (AIMS). An ECG-based method was next developed by Solem et al. (2004) for the detection of acute hypotension which was able to provide information of the patient's propensity to hypotension at an early stage of hemodialysis. In another study conducted by Halkin et al. (2005), seven risk factors were identified as accurate predictors of mortality for cardiogenic shock. According to their research, measurement of baseline left ventricular function was the single most powerful predictor of survival which should be incorporated into risk score models. Recently, multivariable logistic regression modeling techniques was used by Zhang et al. (2007) to develop a model for predicting the occurrence of cardiogenic shock. On the basis of the coefficients in their model, they developed a risk score for the probability of cardiogenic shock.

The presented study concentrates on the detection of AHE and MAPDRs on the basis of ECG signal and ABP waveform measurements. To meet this end, the QRS complexes and end-systolic end-diastolic pulses are first identified using two versions of the MHT algorithm namely as ECGMHT and BPMHT, respectively. Then,

using the obtained SBP and DBP waveforms, MAP trend is specified. Afterwards, in order to smooth the fast fluctuations observed in RR-tachogram and MAP trend, an innovative smoothing algorithm based on piecewise polynomial fitting (PPF) was designed (Figure 1). Fitting N numbers of polynomials sequentially to the original signal and determination of the corresponding coefficients based on BLUE approach (Ghaffari and Homaeinejad, 2008) is the basis of the PPF algorithm operation. In order to consider the mutual influence of parameters on the evaluation of shock probability, a Sugeno adaptive network-based fuzzy inference system-ANFIS is trained using Hasdai et al parameters as input, with appropriate membership functions for each parameter. Using this network, it will be possible to incorporate the possible mutual influences between risk parameters such as heart rate (HR), systolic blood pressure (SBP), diastolic blood pressure (DBP), age, gender, weight and some miscellaneous factors to the calculation of shock occurrence probability. The block diagram of present study is illustrated in Figure 1. Finally, the proposed algorithm is applied to 15 subjects of the MIMIC II Database <http://www.physionet.org/physiobank/database/mitdb/> and <http://www.physionet.org/physiobank/database/slpdb/> and AHE and MAPDRs are consequently detected ($MAP \leq 60$ mmHg with endurance more than 30 min). As a result of this study, MAPDR is realized as a marker of cardiogenic shock. In that, for a sequence of MAPDRs as long as 20 min or more appeared in the MAP trend, there would exist an ensuing high peak with the duration of 3 to 4 min in the probability

of shock diagram which is derived using the risk scoring model developed by Hasdai et al. (2000).

DESCRIPTION OF THE MHT ALGORITHM

From a general point of view, this algorithm consists of 10 stages. In stage (a), using an appropriate bandpass FIR filter, the original ECG signal is filtered and therefore the effects of low frequency noises (motion artifacts) and high frequency noises (device noise) are eliminated. In the stage (b), conventional Hilbert transform is taken from the filtered signal. In the stage (c), according to the Equation (5), signal $y_1(t)$ is entered to a nonlinear function and then the output of this nonlinear function maps the filtered signal $y_0(t)$. In the stage (d), first, only positive values of the signal $y_2(t)$ remain unchanged while the negative values of the signal $y_2(t)$ are mapped to zero. Then the resulted signal is normalized by dividing it to its maximum value. In the stage (e), the signal $y_3(t)$ passes through another nonlinear amplifying function. The (f) routine depicts an adaptive thresholding procedure in which using the mean and the standard deviation of the signal $y_4(t)$, an appropriate value is generated during each interval of the signal $y_4(t)$ for the purpose of comparison. The value of the aforementioned threshold is obtained according to the equation $\tau_j = \mu_j + \alpha \sigma_j$ value. After subtraction of resulted threshold from the signal $y_4(t)$, only positive values are held while negative values are replaced by zero and afterwards, the $y_4(t)$ is multiplied by this nonlinear gain. In the stage (g), using a window which slides sample to sample the maximum value and the corresponding index for each segment is found and other values in the segment are pushed down to zero. Therefore, by sliding this window along the signal, the best local maximum among the other local maxima is obtained. In the stage (h), the resulted signal from stage (g) is divided into identical segments and then a simple local search is performed to find resulted impulses (Figures 2a-f). In this stage, obtained QRS indices are transferred to the original ECG signal and another local search is performed to find the precise position of the R-peak on the unfiltered ECG. After this stage, RR-intervals (RR-tachogram) are obtained and then using two thresholds with low and high values respectively, the complexes making RR-interval abnormal relative to the preceding RR-interval are removed. If threshold is chosen low, the detected QRS complexes set is a compound of normal QRS complexes and PVCs. On the other hand, if the threshold value is chosen high, the detection set almost entirely consists of normal complexes. Lastly, RR-intervals much smaller than the mean RR value are eliminated.

A quadrature filter with the following transfer function is called Hilbert transform which is an all-pass filter that changes the phase of the input signal -90° and has an impulse response of $1/(\pi t)$ (Benitez et al., 2001),

$$G(\omega) = -j \operatorname{sign}(\omega) = \begin{cases} -j & \omega > 0 \\ 0 & \omega = 0 \\ +j & \omega < 0 \end{cases} \quad (1)$$

Therefore, the Hilbert transform of the signal $s(t)$ can be obtained from the following convolution,

$$s_H(t) = s(t) * \frac{1}{\pi t} = \frac{1}{\pi} \int_{-\infty}^{+\infty} \frac{s(\lambda)}{t - \lambda} d\lambda \quad (2)$$

The most significant characteristic of Hilbert transform is its mapping of local maxima and minima values of the original signal to the values crossing of the zero, (Benitez et al., 2001; Natalia et al., 2008). Assume that $y(t)$ represents the original ECG signal and,

$$y_0(t) = y(t) * h_{BP}(t) \quad (3)$$

Where:

$h_{BP}(t)$ = the impulse response of the bandpass FIR filter;

$y_0(t)$ = the output of the filter.

$$y_1(t) = \operatorname{Hilbert} [y_0(t)] \\ t = 0, 1, 2, \dots, n_i - 1 \quad (4)$$

Also assume that the signal $y(t)$ represents an ECG lead in which R-peaks are upward. As can be seen in Figure 2g, a sign change from positive to negative in Hilbert transform of a signal is an indicator of the existence of a local maximum; however, an opposite sign change shows the existence of a local minimum in the signal. Using the following mapping, it would be possible to push down the positive part of Hilbert transform to zero while the negative part is mapped to a constant value.

$$y_2(t) = K_{2mag} y_0(t) \exp \left[\frac{-\lambda_{att}}{2} [1 + \operatorname{sign}(y_1(t))] \right] y_1(t) \quad (5)$$

In which K_{2mag} is the amplification coefficient, $y_0(t)$ is the filtered ECG signal, λ_{att} is the attenuation coefficient, which is a positive value and always $\lambda_{att} \geq 1$. The $\operatorname{sign}(\cdot)$ operator is the sign function and $y_1(t)$ is the Hilbert transform of the filtered signal. According to Equation 5, it can be realized that for a negative value of $y_1(t)$,

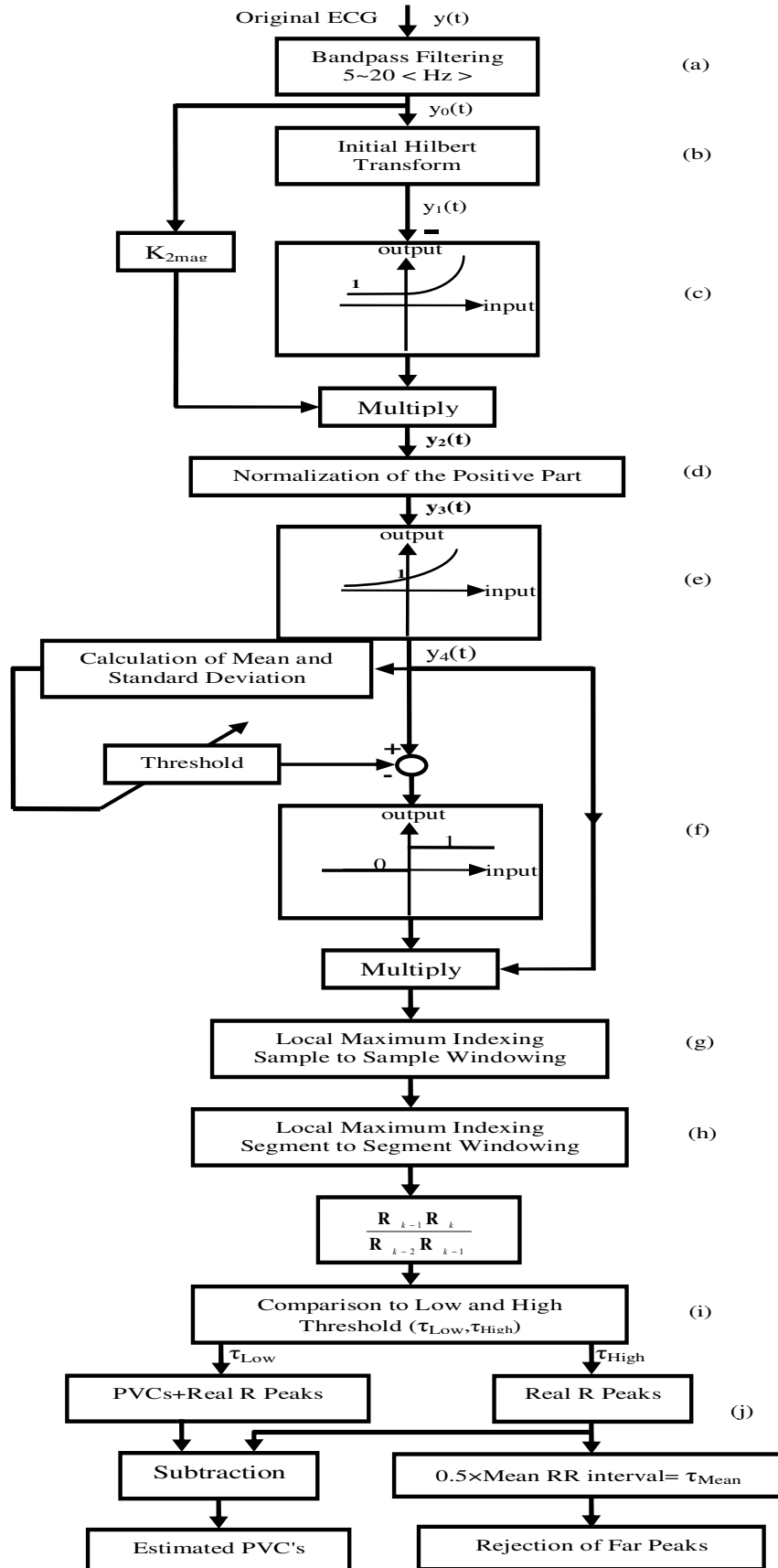


Figure 2. The block diagram of the MHT algorithm.

$y_2(t) = K_{2mag} y_0(t) \exp(0) = K_{2mag} y_0(t)$ and the output would be the amplified version of the filtered signal. However, for positive values of $y_1(t)$, $y_2(t) = K_{2mag} y_0(t) \exp[-\lambda_{att} y_1(t)] \approx 0$. Thus, for negative values of Hilbert transform, the filtered signal will be amplified and for positive values of Hilbert transform, the filtered signal will be mapped near zero. In the next step, using another nonlinear function, the negative values of the signal $y_2(t)$ are eliminated, as follows:

$$y_3(t) = K_{3mag} [1 + \text{sign}(y_2(t))] y_2(t) \quad (6)$$

Where: K_{3mag} represents the amplification coefficient.

According to this equation, for a negative value of $y_2(t)$, the signal $y_3(t)$ will be equal to zero; however, for positive values of $y_2(t)$, the signal $y_3(t)$ will be amplified with the proportional factor K_{3mag} . Afterwards, the signal $y_3(t)$ is normalized and then re-amplified to define a proper subject-independent thresholding on the signal, as follows:

$$y_4(t) = \exp\left[\frac{y_3(t)}{\max(y_3(t))}\right] \quad (7)$$

Where $\max(y_3(t))$ represents the maximum value of the signal $y_3(t)$.

Design of adaptive thresholding on the signal $y_4(t)$

Due to the variability of the morphology of QRS complexes in cases of arrhythmia, it will not be possible to detect all R-peaks using a fixed threshold value. For instance, if the threshold value is rather large relative to unity (unity is the minimum value of the signal $y_4(t)$) therefore, the QRS complexes with a small $y_4(t)$ value, will be located beneath the threshold line and consequently will not be detected. On the other hand, for values of threshold highly close to unity, some waves will be detected in addition to QRS complexes which will lead to a decrease in the algorithm accuracy, even if an improperly-detected QRS elimination algorithm is

implemented. Accordingly, it seems that an adaptive thresholding is necessary and the algorithm would be more efficient. Suppose that the signal $y_4(t)$ is divided into N number of identical segments, with the values of μ_j and σ_j , respectively for mean value and standard deviation of the signal segment in the j th interval ($j = 1, 2, \dots, N$). For a threshold of $\tau_j = \mu_j + \alpha \sigma_j$, where α is the adjustment coefficient ($0 < \alpha \leq 6$), one can calculate the corresponding suitable comparison threshold of each sample of the signal $y_4(t)$ in each interval of $y_4(t)$. Thus, variability in the amplitude of the signal $y_4(t)$, even in case of large variation, will not cause significant errors in the proposed detection algorithm.

Sample to sample windowing: Selection of the best local minimum

In this step, a window with an appropriate length of samples is selected and is slid on the signal $y_5(t)$ from one sample to the next. Each time, the maximum value in the window and the corresponding index is calculated and all other points in the window are padded by zero. If moving forward, the new maximum entered the window is larger than the previous one, the previous maximum will be replaced by zero and the current maximum will play as a new QRS candidate. Finally, the output of the window will be called as the best candidate for R-peak of QRS complex.

Accordingly, using the calculated threshold, the signal $y_5(t)$ can be obtained from signal $y_4(t)$ as follows:

$$y_5(t) = \begin{cases} y_4(t) & y_4(t) \geq \tau(t) \\ 0 & y_4(t) < \tau(t) \end{cases} \quad (8)$$

Eventually, after applying a local search to the entire resulted signal, the proper candidates of QRS complexes will be obtained.

Elimination of improperly-detected waves

In order to eliminate the QRS complexes with abnormal time distances from each other, suppose that the index k represents the k -th R-wave in the signal. Consequently, using a hypothesis test with the following test ratio:

$$L_R = \frac{R_{k+1} - R_k}{R_k - R_{k-1}} \quad (9)$$

And a decision rule based on the following criterion

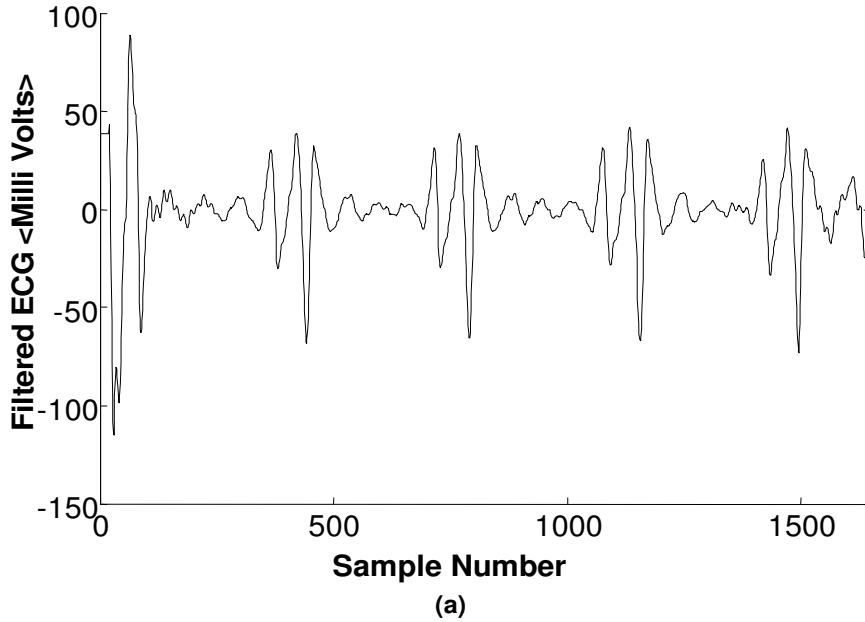


Figure 3a. Graphical representation of the performance of MHT algorithm in the detection of QRS complexes; filtered ECG signal.

$$\delta = \begin{cases} 1 & L_R \geq \tau_R \\ 0 & L_R < \tau_R \end{cases}, \quad \begin{matrix} 1 \equiv \text{Holding} R_{k+1} \\ 0 \equiv \text{Rejecting} R_{k+1} \end{matrix} \quad (10)$$

The $(k+1)$ th R-wave with abnormal distance from the preceding R-wave will be eliminated. It should be noted that in Equations (9) and (10) τ_R is the rejection ratio and L_R is the decision ratio. In order to detect PVC beats, the factor τ_R should be chosen between 0.45 and 0.55 ($0.45 \leq \tau_R \leq 0.55$). However, for the values of τ_R between 0.55 and 0.70 ($0.55 \leq \tau_R \leq 0.70$) more accurate results will be obtained for R-wave detection. Finally, to remove much improperly-detected R-waves, it is assumed that the time sequence of RR-intervals (RR-tachogram) has a mean value μ_C and standard deviation σ_C . Thus, if the equation $(R_k - R_{k-1}) \leq \mu_C + 3.5\sigma_C$ is held, the R_k peak will be rejected. The schematic block diagram of the MHT algorithm is depicted in Figure 2. It is also shown in Figure 3 how the developed algorithm works to detect QRS complexes.

Design of piecewise polynomial fitter (PPF)

The design of piecewise polynomial fitter (PPF) is based on the least squares method. In the PPF algorithm, the original signal is first divided into identical segments.

In the next step, a p th-order polynomial ($3 \leq p \leq 15$, this interval is obtained empirically after numerous simulations) is fitted to each signal segment in the corresponding windows. Next, the discontinuities in the beginnings and the ends of the intervals are eliminated using some simple calculations. The PPF algorithm has acceptable capability in cases of noise with non-stationary variance, low signal to noise ratios, and colored noise. In this section, the design procedure of the PPF algorithm and the corresponding implementation method is first described and the related performance characteristics are then explained.

The principle of least squares

The principle of least squares extensively has been studied in systems identification (Söderstrom and Stoica, 1989) and estimation theories (Kay, 1979) textbooks. Consider the k th segment of a signal with the length W_N such as $\{y(t) | t = 1 + (k-1)W_N : kW_N\}$. A typical p th-order polynomial is supposed to be fitted to this signal segment as follows:

$$\hat{y}_k(t) - y_{ok} = \sum_{n=1}^p a_{nk} (t - t_{ok})^n \quad (11)$$

Where:

$\hat{y}_k(t)$ = the estimation of the original signal in the k th

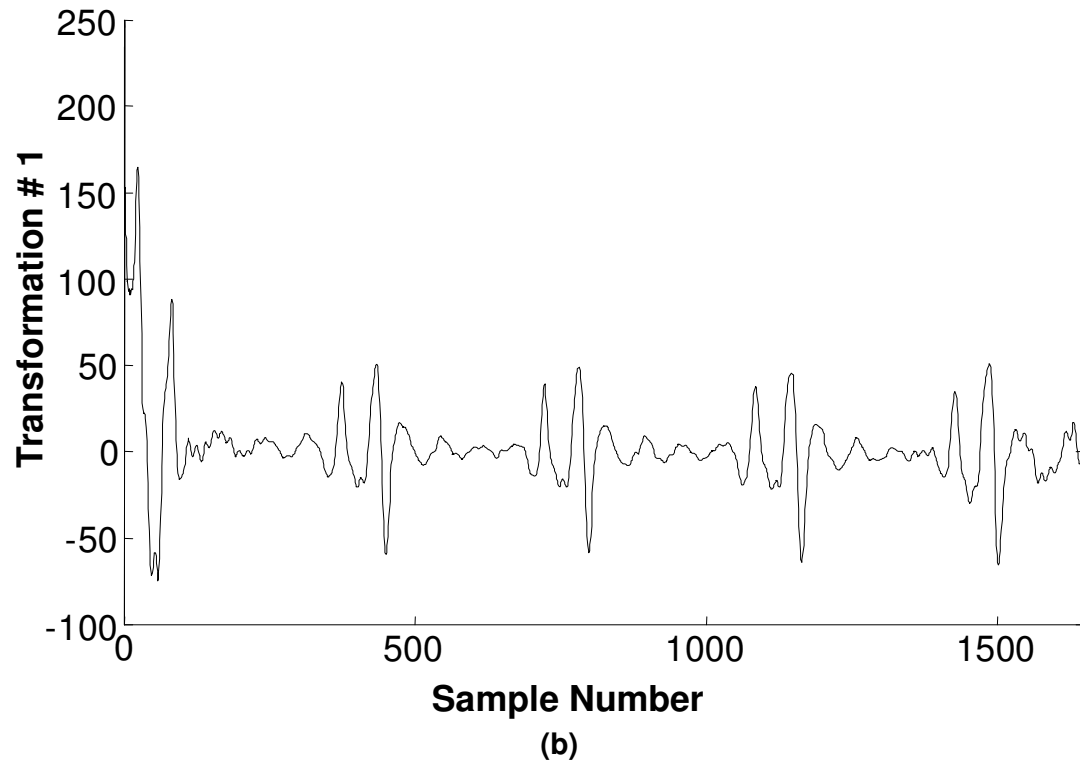


Figure 3b. Graphical representation of the performance of MHT algorithm in the detection of QRS complexes; conventional Hilbert transform.

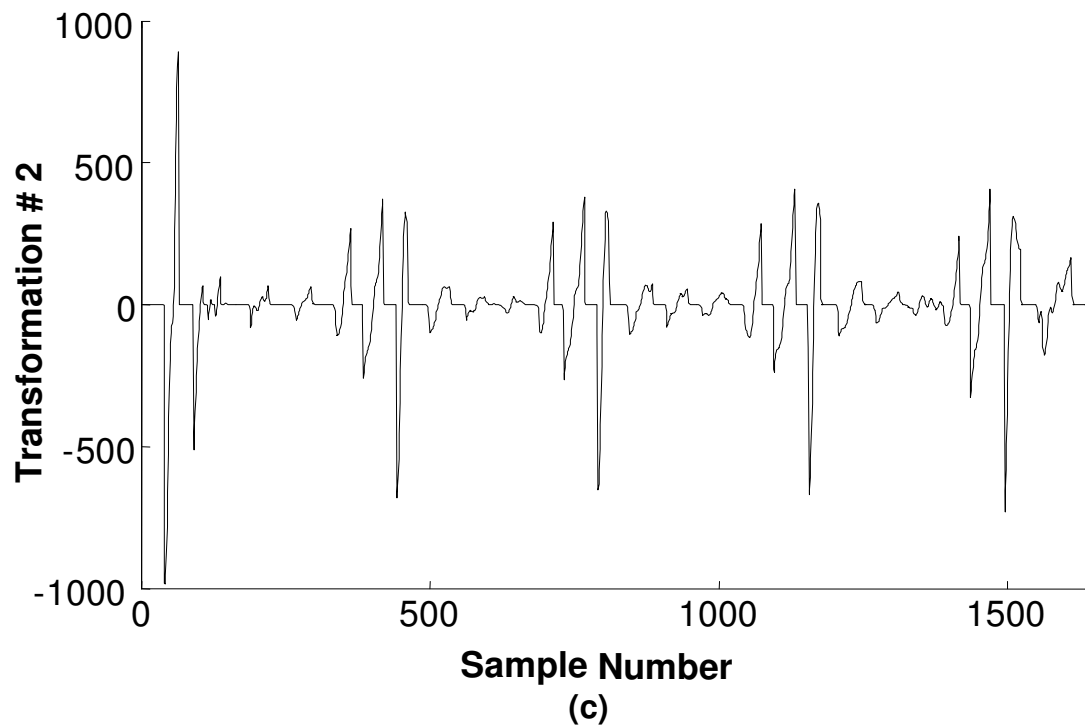


Figure 3c. Graphical representation of the performance of MHT algorithm in the detection of QRS complexes; nonlinear mapping according to Equation (5).

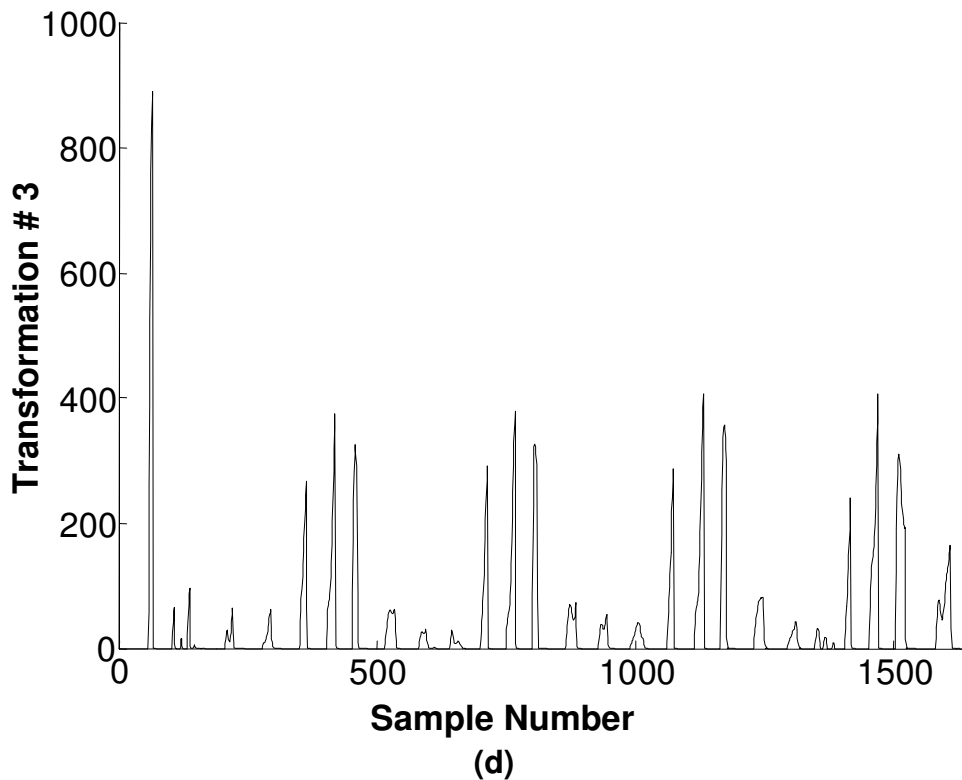


Figure 3d. Graphical representation of the performance of MHT algorithm in the detection of QRS complexes; padding zeros instead of negative values in signal obtained from previous section.

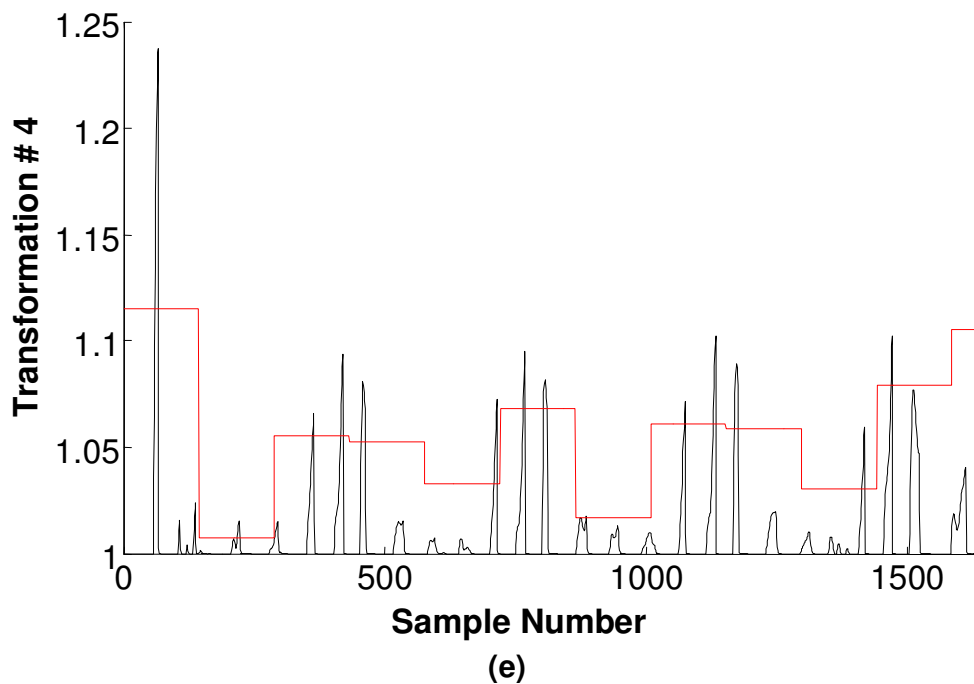


Figure 3e. Graphical representation of the performance of MHT algorithm in the detection of QRS complexes; normalization and exponentially amplification of the preceding signal and application of the adaptive thresholding

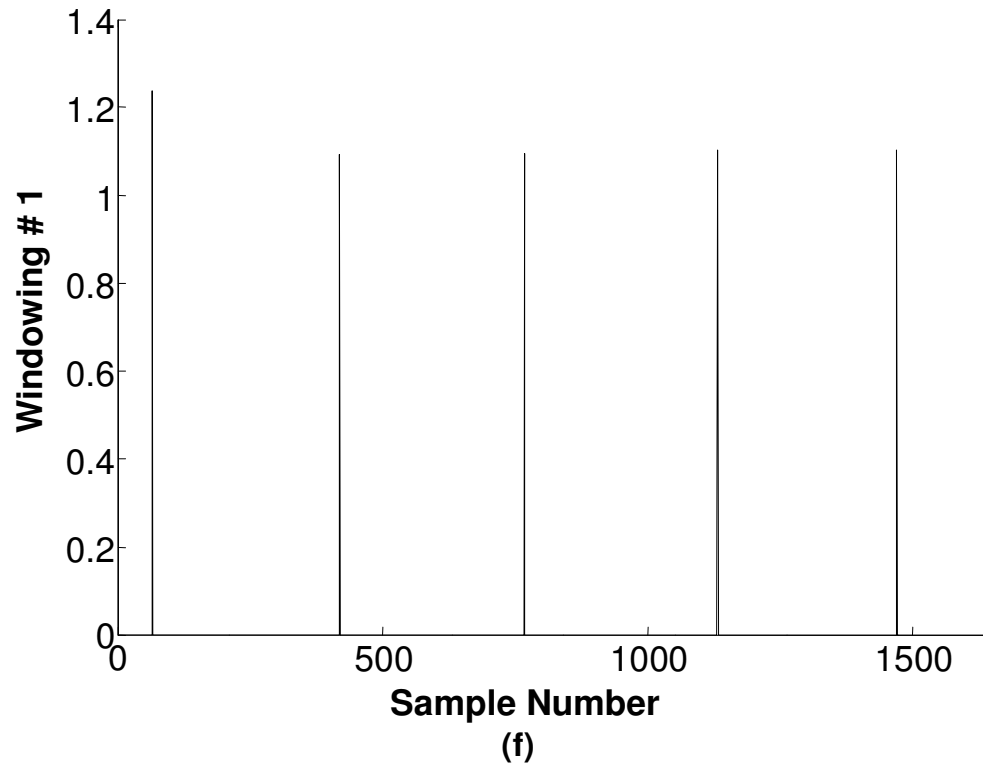


Figure 3f. Graphical representation of the performance of MHT algorithm in the detection of QRS complexes; application of the sliding window to form the impulses originated from the best local maxima candidates.

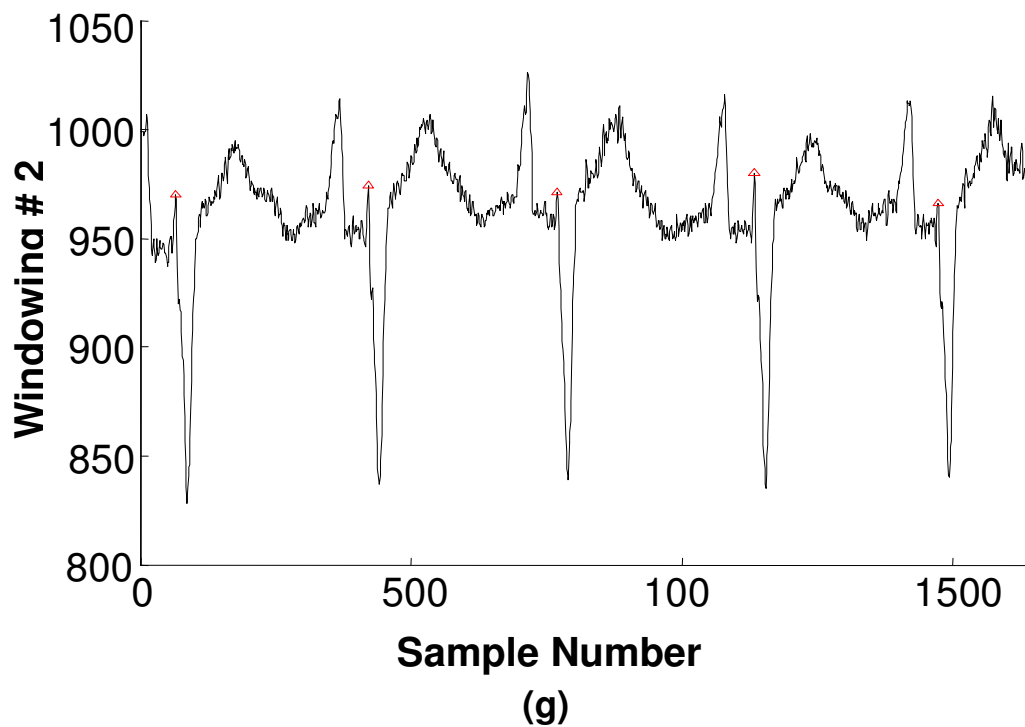


Figure 3g. Graphical representation of the performance of MHT algorithm in the detection of QRS complexes; application of a local search to the original signal centered on impulse indices obtained from stage (f).

interval;

y_{0k} = the initial value of the interval;

t_{0k} = the start time of the interval, and

a_{nk} represents the polynomial coefficients which should be estimated using BLUE algorithm.

Assuming the number of samples for each signal segment to be W_N , the following observation vector and time vector can be obtained for the k th segment of the signal

$$\begin{cases} \mathbf{y}_{obs,k} = \mathbf{y}[(1+(k-1)W_N):kW_N] \\ \mathbf{t}_{obs,k} = \mathbf{t}[(1+(k-1)W_N):kW_N] \end{cases} \quad (12)$$

Where $\mathbf{y}^{[m:n]}$ represents the elements number m to n of a supposed vector \mathbf{y} .

Generally, in order to apply the BLUE algorithm to the problem, the observation and linear regression vectors must be in column and row formats, respectively. The

observation vector \mathbf{Y}_k and time vector \mathbf{T}_k in the k th interval are obtained using Equation (12) as follows

$$\begin{aligned} (\mathbf{Y}_k)_{W_N \times 1} &= \mathbf{y}_{obs,k} - y_{0k} \\ (\mathbf{T}_k)_{W_N \times 1} &= \mathbf{t}_{obs,k} - t_{0k} \end{aligned} \quad (13)$$

Where y_{0k} and t_{0k} are the initial values of the k th interval and should be chosen as to the continuity of the entire estimated signal is guaranteed.

In order to determine the matrix consisting of linear regression vectors, the time column vector $(\mathbf{T}_k)_{W_N \times 1}$ is substituted in the following matrix

$$\Phi_k = [\mathbf{T}_k, (\mathbf{T}_k)^{*2}, \dots, (\mathbf{T}_k)^{*p}] \quad (14)$$

Where the operator $(\cdot)^{*m}$ increases each element of the matrix \mathbf{T}_k to the power of m . Suppose that in the observation vector \mathbf{Y}_k , the signal is embedded into an additive noise with covariance matrix Ω_k . If so, it can be shown that the best linear unbiased estimation of unknown parameters in the presence of correlated noise is as follows (Soderstrom and Stoica, 1989)

$$\theta_k = (\Phi_k^T \Omega_k^{-1} \Phi_k)^{-1} \Phi_k^T \Omega_k^{-1} \mathbf{Y}_k \quad (15)$$

In which, θ_k includes the parameters of the polynomial in an ascending fashion, that is, $\theta_k = [a_{1k}, a_{2k}, \dots, a_{pk}]^T$. The details to derive this equation as well as the corresponding exhaustive explanation of this type of estimation can be found in identification textbooks (Söderström and Stoica, 1989; Kay, 1979). Presenting a simple example, it is shown how to apply the continuity condition to the beginning and end of each interval. Consider a sequence consisting of 17 samples with the window length $W_N = 12$ as depicted in Figure 4.

Improperly-detected QRS elimination algorithm is in this figure, the solid line represents the original signal which should be estimated by the PPF algorithm and the dashed lines illustrate polynomials fitted to the signal in each segment. As can be observed in this figure, the estimated signal is not appropriately fitted to the original signal at end point A (end effect 1). To solve the problem, it is assumed that the corresponding polynomial of each interval is fitted to W'_N number of samples, where $W'_N = W_N + W_{aug}$, and W_{aug} is the number of samples borrowed from the next adjacent window augmented to the vector \mathbf{T}_k . According to Equation (12), vectors $\mathbf{y}_{obs,k}$ and $\mathbf{t}_{obs,k}$ are obtained as follows

$$\begin{cases} \mathbf{y}_{obs,k} = \mathbf{y}[(1+(k-1)W_N):kW_N + W_{aug}] \\ \mathbf{t}_{obs,k} = \mathbf{t}[(1+(k-1)W_N):kW_N + W_{aug}] \end{cases} \quad (16)$$

In this way, the polynomial parameters are determined from Equation (15) and the corresponding signal in this interval can be estimated as follows:

$$\mathbf{T}_k = \mathbf{t}[(1+(k-1)W_N):kW_N + 1] - t_{0k} \quad (17)$$

$$\Phi_k = [\mathbf{T}_k, (\mathbf{T}_k)^{*2}, \dots, (\mathbf{T}_k)^{*p}]_{(W_N+1) \times p} \quad (18)$$

$$\hat{\mathbf{y}}(t) = \Phi_k \theta_k + y_{0k} \quad (19)$$

Applying this method, the end effect 2 (end point B) is arisen out of the interval. However, samples only from the beginning to the end of segment (W_N) are considered as the estimated signal. Therefore, the end effects are eliminated.

It should be noted that the signal in this interval is estimated using a rather high-order polynomial which has low generalization power for the estimation in endpoints.

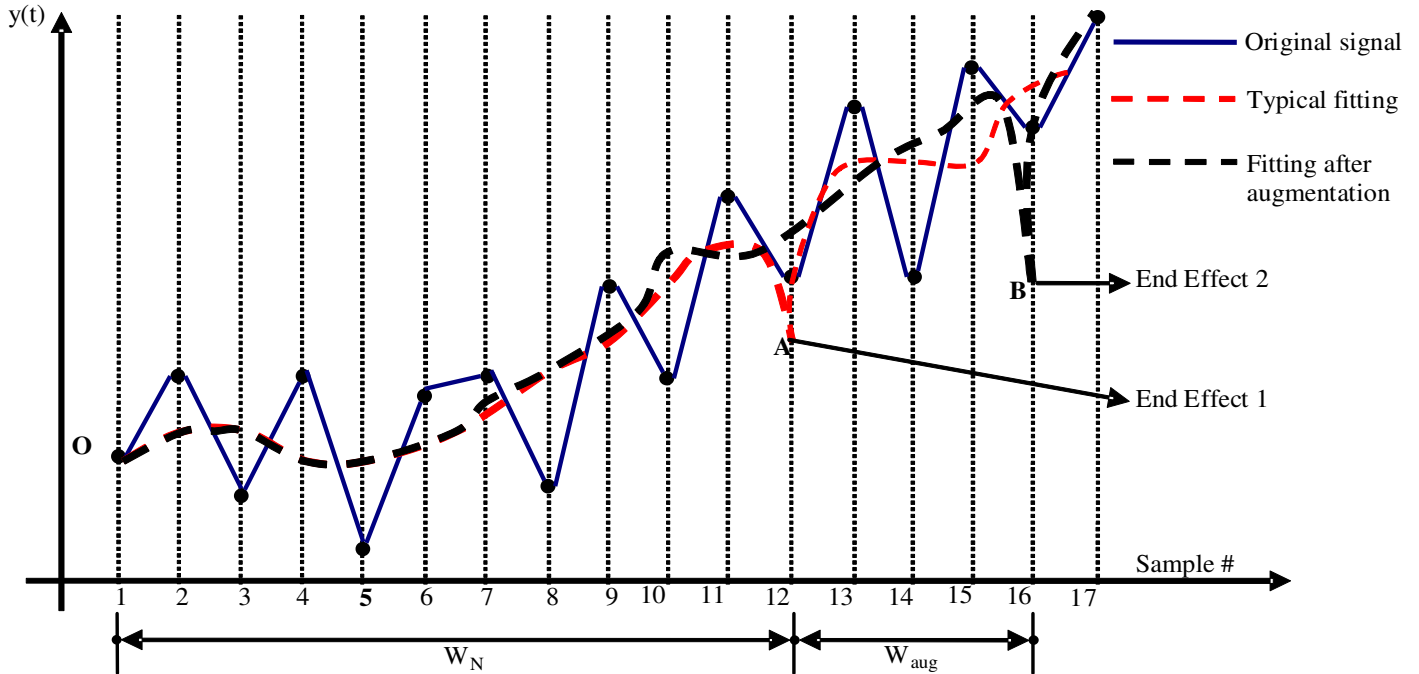


Figure 4. Schematic representation of end effects in the PPF algorithm and extra samples augmentation.

Choosing some samples from the interval $k+1$, to proceed the last sample of the interval k , results in more accurate estimation for endpoint and consequently a smoother estimation is obtained for the original signal in the interval k . The last point of the interval k and the corresponding time will be used as the initial conditions for the next interval, $k+1$. That is

$$\begin{cases} y_{0(k+1)} = \hat{\mathbf{Y}}_k(\text{end}) \\ t_{0(k+1)} = \mathbf{T}_k(\text{end}) \end{cases} \quad (20)$$

Finally, in order to conduct estimation in the interval $k+1$, the linear regression matrix and the observation vector should be obtained from Equation (19) and the first elements in the vectors $\mathbf{t}_{obs,(k+1)}$ and $\mathbf{y}_{obs,(k+1)}$ should be replaced by $y_{0(k+1)}$ and $t_{0(k+1)}$, respectively.

Generally, it should be noted that the window length W_N depends upon the sampling frequency, frequency contents of the original signal, the order of the polynomial and noise power. After fulfillment of numerous simulations, it is empirically concluded that this performance would be highly improved if the following criterion is used.

$$W_N = \lambda \min \left\{ \frac{1}{4} F_s, 3f_{dom}, 15p \right\} \quad (21)$$

Where:

F_s represents the sampling frequency,

f_{dom} is the largest frequency existing in the signal, and p is the order of the polynomial.

Also, λ is a proportion coefficient which varies between 1 and 1.5 ($1 \leq \lambda \leq 1.5$) and depends on the approximate standard deviation of the noise.

In this study, for the values of noise standard deviation less than 4 ($\sigma_N < 4$), λ is set to 1 ($\lambda=1$) and for the values of noise standard deviation more than 4 ($\sigma_N > 4$), it was considered equal to 1.5 ($\lambda=1.5$).

Cardiogenic shock and risk scoring model

Cardiogenic shock is a certain state in which slight systemic cardiac output leads to tissue hypoxia. For the values of cardiac index less than or equal to 2.2 liter/min/m² (or 1.8 liter/min/m² according to physiologists) cardiogenic shock will occur. From blood pressure perspective, a systolic blood pressure less than 80 or 90 mmHg can be a symptom of shock syndrome. However, it is proven that hypotension is not the only cause of shock occurrence. The hemodynamic parameters which contribute significantly to the detection or prediction of

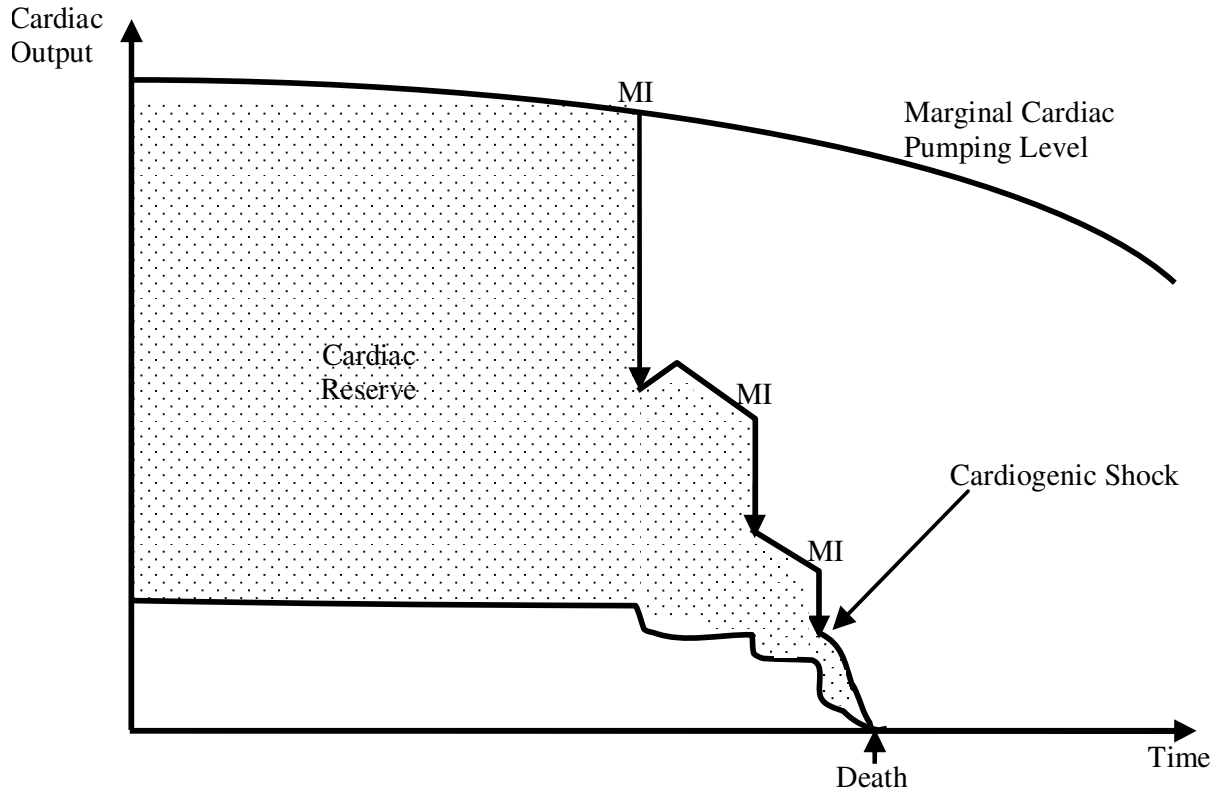


Figure 5. The diagram of cardiogenic shock occurrence after cumulative MIs showing deterioration of cardiac pumping capability (Hasdai et al., 2008).

shock are namely as heart rate, right atrial pressure, right ventricle systolic/diastolic pressure, pulmonary artery pressure, left atrial pressure, left ventricle systolic/diastolic pressure, aortic pressure, cardiac output, cardiac index, stroke volume, left ventricle diastolic volume, ejection fraction, systemic resistance, total pulmonary resistance, stroke work index of the left ventricle, and baseline cardiac power out. Generally, considerable decrease will occur in the systemic tissue perfusion during cardiogenic shock. The main consequences of cardiogenic shock include renal failure, changes in pulmonary function, changes in the skeletal muscle, dysfunction in the gastrointestinal system, decrease in blood pressure and blood volume, and damages to the brain. The schematic diagram of the cardiogenic shock is illustrated in Figure 5, in which successive MI cause the cardiac pumping level descend to the below of rest baseline. In this way, cardiogenic shock occurs which can rapidly lead to death (Hasdai et al., 2008).

In this section, a shock predictor model (Hasdai et al., 2000) is introduced in which factors such as age, heart rate, SBP, DBP, weight and some other clinical features namely as miscellaneous factors are incorporated. In the first step, based on clinical data and significance of the factor under study, a score is allocated to each feature.

For instance, age is a variable strongly increasing the probability of cardiogenic shock, or mean arterial pressure (MAP) which is derived from SBP and DBP and considerably is associated with the occurrence of cardiogenic shock. Therefore, a high score should be allotted to these factors. Afterwards, a total score is calculated as the sum of the scores assigned to each factor. Finally, it would be possible to predict the probability of cardiogenic shock for the patient under consideration. As a case in view, consider a 71-year-old 60-kg female with a history of hypertension, who presents with a systolic blood pressure of 126 mmHg, a diastolic blood pressure of 64 mmHg, and a heart rate of 123 beats/min. According to the model of Hasdai et al., this patient would have a total score of $37+17+39+5+10+5+8+17+3+2+5=148$. This score corresponds to predicted probability of 30% for cardiogenic shock (Hasdai et al., 2000).

Computer implementation of Hasdai et al model

For Computer Implementation of Hasdai et al Model, an adaptive network-based fuzzy inference system (ANFIS) is trained using the information obtained from the their original work (Hasdai et al., 2000). The purpose of using

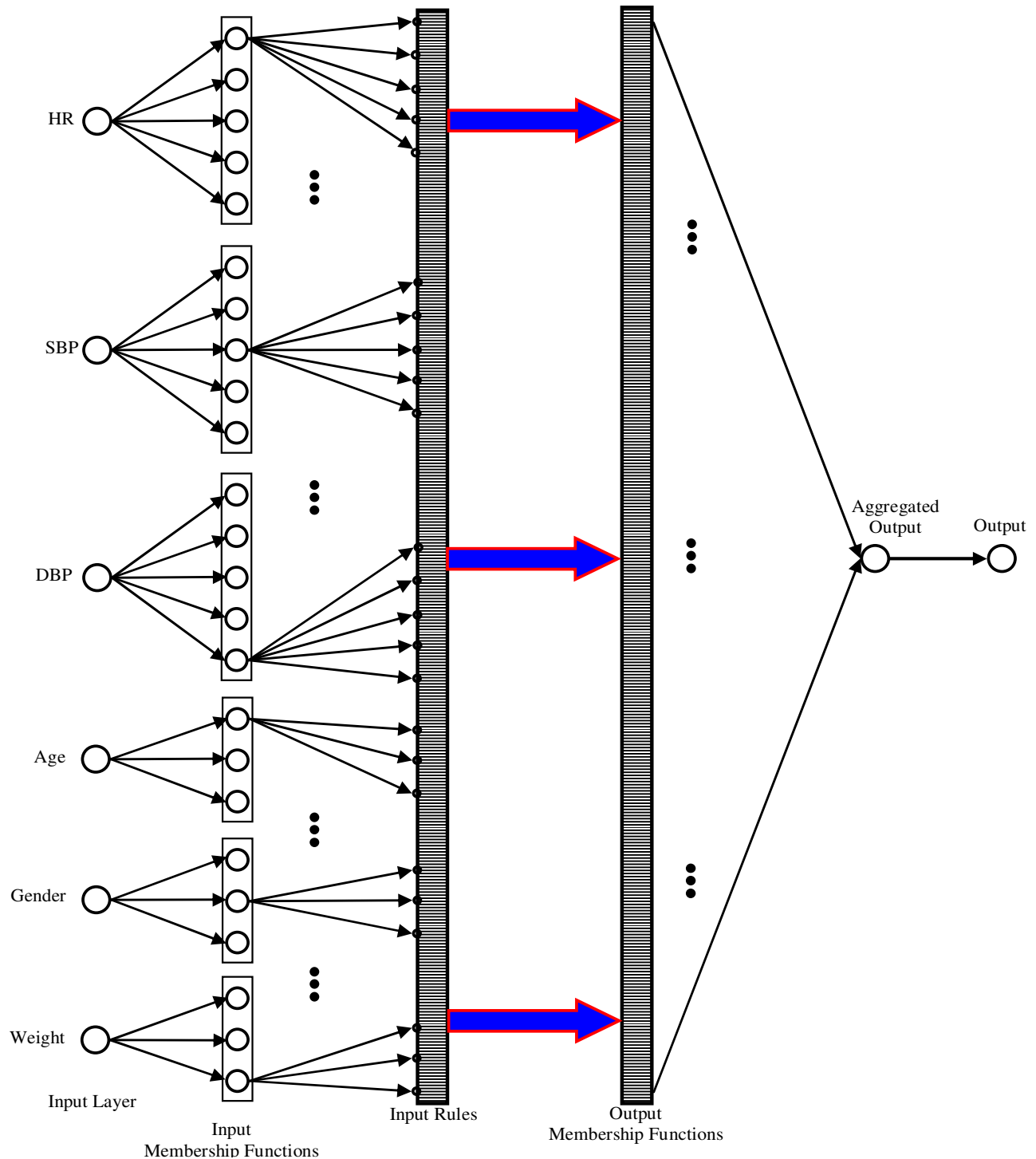


Figure 6. The ANFIS structure used for cardiogenic shock predictor based on HR, SBP, DBP, age, gender and weight.

ANFIS was to consider the mutual influence of parameters in the evaluation of error probability, an ANFIS network is implemented. Using this network, it will be possible to incorporate the possible mutual influences between risk parameters to the calculation of shock occurrence probability. Adaptive neuro-fuzzy networks

are actually fuzzy inference systems which are translated to a neural network language and using the neural network features, the actual system is trained based on the input-output data and then turned into a fuzzy model. More details about ANFIS can be seen at (Jang 1993).

According to Figure 6, inputs such as HR, SBP, DBP,

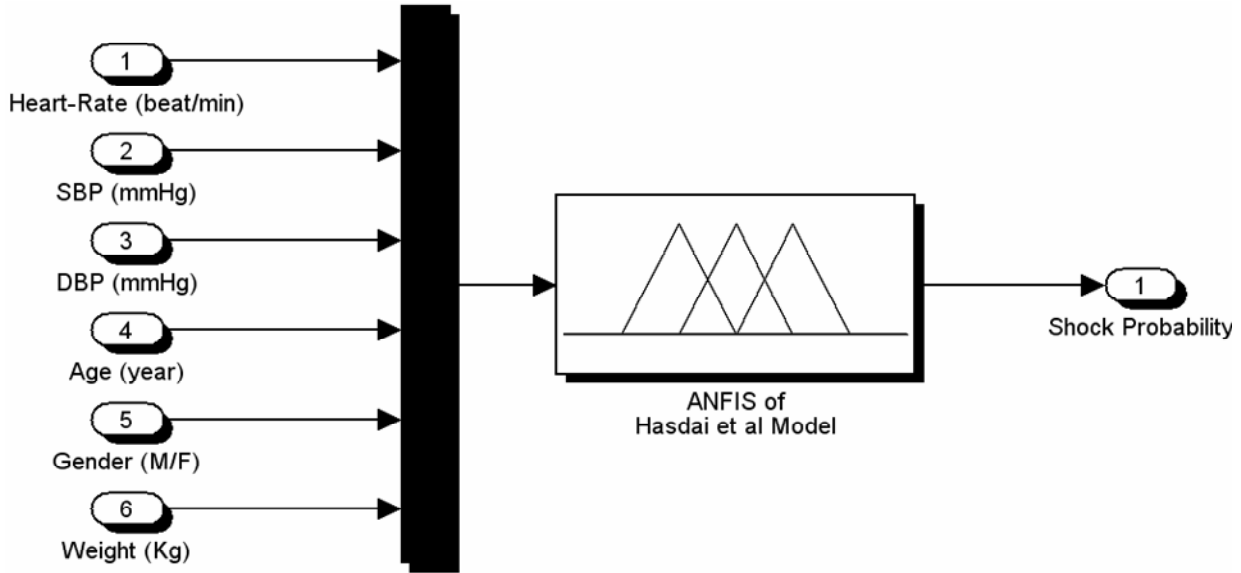


Figure 7. SIMULINK circuit used to implement the trained ANFIS with marked input and outlet ports.

age, gender, and weight are included in the first layer and incorporated to fuzzy membership functions. The outputs of neurons are the membership values of inputs in fuzzy values. This part of the neuro-fuzzy network is equivalent to the IF part of the fuzzy inference system. In the Input Rules Layer, resulted membership values are passed through a T-norm and the firing strength of each rule is determined. In the output membership layer, using the final relationships, the output of each IF-THEN rule is determined. For each of the parameters of HR, SBP, and DBP, five Gaussian memberships are considered with a Sugeno Difuzzification algorithm. For all other parameters of the Hasdai et al model, 3 triangular memberships are selected as to less computational burden and complexity is achieved. The structure of this network is illustrated in Figure 5.

The resulted ANFIS model is used in a SIMULINK environment according to Figure 7 to calculate the risk of cardiogenic shock occurrence. As already stated, the variable describing shock in the Hasdai et al. model can be obtained using an equation similar to the following

$$X_{TOT} = X_{AGE} + X_{HR} + X_{SBP} + X_{DBP} + X_{WGT} + X_{MIL} + X_{TRT} + X_{KLP} + X_{MSC} \quad (22)$$

More details about the Hasdai et al. risk score model can be found in (Hasdai et al., 2000). As understood from Equation 22, the total sum of scores will yield the shock overall index and using a final mapping, the percentage of the probability of shock occurrence can be calculated (Hasdai et al., 2000).

Names of records extracted from Physionet database are presented in Table 1. From the parameters needed in Hasdai et al. model, HR, SBP, DBP, age and gender are available. However, other parameters such as treatment,

MI location, Killip class, weight, and other miscellaneous factors are not known and therefore are set equal to average values, according to Table 1. In Figure 8, the parameterized Gaussian and triangular membership function are illustrated. According to this Figure, each Gaussian membership function is specified by two parameters (μ, σ) and each triangular membership function is determined by three parameters (μ_L, μ_C, μ_R).

After training of an ANFIS network with the structure shown in Figure 5 using MIMICII database according to Table 1 specifications, the parameters of each membership of the ANFIS structure are obtained as shown in Table 2.

Finding MAPDRs using PPF algorithm

Since MIT-BIH Database includes long time signals (more than 30 h), the outputs of BPMHT and ECGMHT algorithms are averaged in one-minute intervals. If so, the size of data to be processed will be 1/125 of the size of original data, (the sampling frequency of MIMIC II Database is 125 Hz). Finally, MAPDR calculations are conducted using the average data.

In order to find MAPDRs, a window with the length W_{DR} is first slid sample to sample on the smoothed averaged waveform $Y_{bp,sm}$ obtained from PPF algorithm that is, $Y_{bp,sm} = PPF(Y_{bp,orig})$. The MAP waveform $Y_{bp,orig}$ is calculated using SBP and DBP pulses, as follows, (Guyton 1996)

$$Y_{bp,orig} \approx \frac{Y_{SBP} + 2Y_{DBP}}{3} \quad (mmHg) \quad (23)$$

Table 1. Specifications of the subjects under study obtained from MIMIC II Database. Due to the lack of sufficient clinical data, treatment, MI location and Killip Class are selected as to the corresponding risk scores are equal to zero.

Miscellaneous grade	Killip class	MI Location	Treatment	# of mean samples	Record # (gender, age)
10	I	Other	TPA	22143	s21775 (M-80)
13	I	Other	TPA	24704	s20658 (F-72)
13	I	Other	TPA	8287	s22466 (F-78)
10	I	Other	TPA	4294	s05336 (M-45)
13	I	Other	TPA	17506	s06349 (F-89)
10	I	Other	TPA	10025	s08718 (M-84)
10	I	Other	TPA	5880	s20794 (M-84)
10	I	Other	TPA	11506	s24799 (M-66)
13	I	Other	TPA	7410	s26318 (M-70)
10	I	Other	TPA	14412	s14204 (F-84)
10	I	Other	TPA	15717	s25699 (M-39)
10	I	Other	TPA	6487	s07125 (M-51)
13	I	Other	TPA	18804	s19208 (F-79)
13	I	Other	TPA	16042	s12821 (F-77)
10	I	Other	TPA	2898	s06637 (M-79)

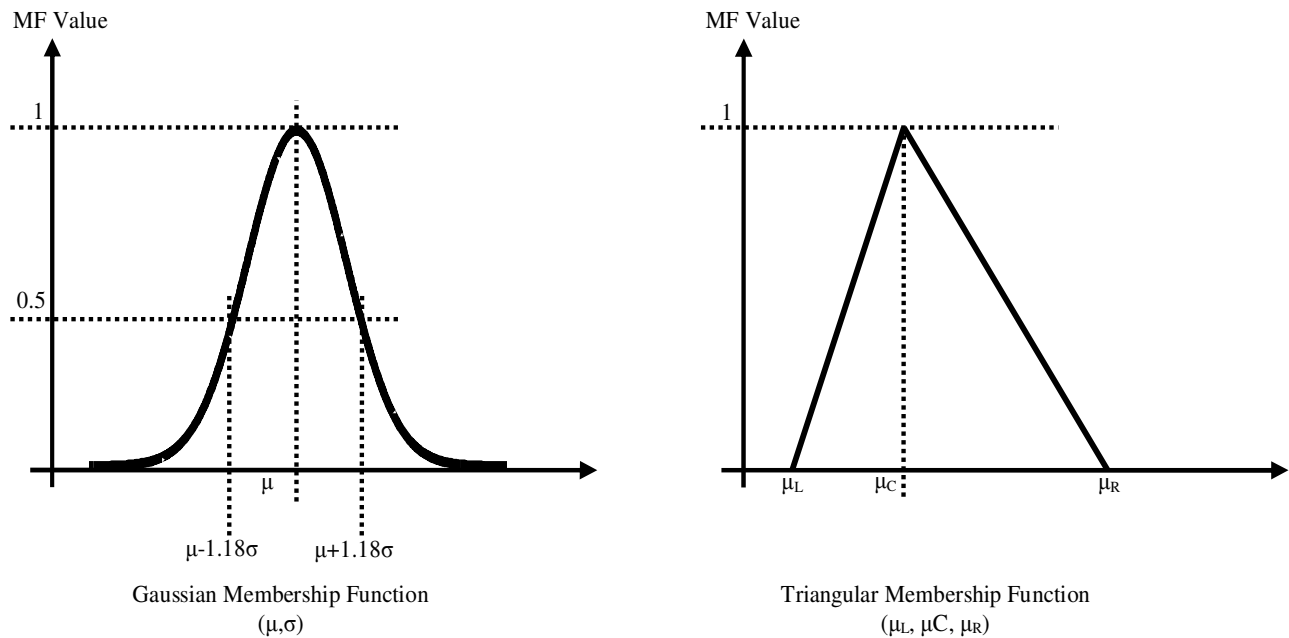


Figure 8. Parameterization of Gaussian and triangular membership functions.

Where Y_{SBP} and Y_{DBP} are SBP and DBP vectors.

The window length W_{DR} is equal to the number of samples long as 30 min. Each time, the drop index (DI), MAPDR, is calculated as follows: First, the signal segment in the k th window is obtained as:

$$Y_{segk} = Y_{b\beta sm}(k:k+W_{DR}) \tag{24}$$

In the next step, the derivative of the vector $Y_{seg,k}$ is calculated with respect to time as follows:

$$\dot{Y}_{seg,k} = diff(Y_{seg,k}) \tag{25}$$

Where the operator $diff(\cdot)$ represents the difference between the present sample and the previous one. The

Table 2. Memberships parameters of the ANFIS structure obtained after training (MF:Membership function, Gss: Gaussian MF, Tra: Triangular MF).

MF#5 type parameters	MF#4 type parameters	MF#3 type parameters	MF#2 type parameters	MF#1 type parameters	Variable/parameter (Range)
Gss(251.2841,18.5647)	Gss(233.5789,24.6312)	Gss (219.8417,45.2966)	Gss (104.0193,23.8715)	Gss (48.1514,21.2317)	HR [40 - 260]beats/min
Gss (279.8637,18.2849)	Gss (251.7119,23.3216)	Gss (227.0328,45.6217)	Gss (101.3261,21.2519)	Gss (74.9817,19.1744)	SBP [80 - 280] mmHg
Gss (191.9122,15.2361)	Gss(186.5611,20.1713)	Gss(154.4349,19.6438)	Gss (97.1583,21.4567)	Gss (44.2567,14.6494)	DBP [40 - 200] mmHg
---	---	Tra (70.1658,81.0429,92.6657)	Tra(44.0741,58.3219,73.8719)	Tra (14.2316,25.5469,49.1799)	AGE [20 - 90] years
---	---	Tra (1.3383,1.4348,1.6524)	Tra (1.2759,1.6949,1.8927)	Tra(0.5728,1.7149,2.3327)	GENDER(Male, Female)
---	---	Tra (171.0561,198.5255,264.9145)	Tra (94.5847,147.4595,189.1541)	Tra (37.5121,61.2353,101.5418)	WEIGHT [40 - 220] Kg

aim of this study is to detect intervals with MAP at or below 60 mmHg descending continuously. To meet this end, all samples of the vector $\dot{Y}_{seg,k}$ in a window are summed up. If this total sum is always negative when sliding the window forward, it would be a marker of MAPDR. On the other hand, an increase in the total sum indicates an ascending trend for MAP. Therefore,

$$DI(k) = \sum_{n=1}^{W_{DR}} \dot{Y}_{seg,k}(n), \quad MAP \leq 60 \text{ mmHg} \quad (26)$$

From the resulted signal DI, negative parts with high duration should be highly considered. Thus,

$$MAPDR = 0.5[1 - sign(DI)] \quad (27)$$

Where the index MAPDR represents a signal with the value of 1 for MAPDR and zero for ascending trend in MAP signal.

If the drop index descends continuously for 90% of the window length when moving forward, a dropping regime will be assigned to that specific period of time.

Normalization of data

Suppose that the supposed vector X has sample

mean μ and sample variance σ^2 , the normalized vector X_{Norm} that has zero mean and unit variance is obtained from the following simple transformation

$$X_{Norm} = \frac{X - \mu}{\sigma} \quad (28)$$

Normalization of shock probability diagram helps us obtain a comprehensive comparative criterion for all subjects.

RESULTS AND DISCUSSION

Implementation of MHT algorithm to ECG signal (ECGMHT)

Numerous databases with different sampling frequencies and signal to noise ratio are used in this study to validate the performance of the proposed detection algorithm. To validate the QRS detection and delineation algorithm, MITDB ($F_s = 360\text{Hz}$), TWADB ($F_s = 500\text{Hz}$), EDB ($F_s = 250\text{Hz}$), QTDB ($F_s = 250\text{Hz}$) and also high resolution Holter data (MEDSET[®]-1000Hz, 3-Channel, 32-bits) which contain annotation files are used (CHECK#0). It should be noticed that in confusing situations, results were delivered to the cardiologist and accordingly, the detection

algorithm was revalidated (CHECK#1). In cases of QRS with very abnormal morphologies, the results were also checked by some residents (CHECK#2).

The results of the application of the MHT method are shown in Tables 3 to 7, with the average values of 99.80 and 99.85% for sensitivity and positive prediction, respectively. The false negative (FN) occurs when the algorithm fails to detect a true beat (actual QRS) conducted in the corresponding annotation file of the MIT-BIH record and a false positive (FP) indicates a false beat detection. Sensitivity (Se), positive prediction (P+), (Benitez et al., 2001), are calculated straightforwardly as follows:

$$\text{Sensitivity (\%)} = \frac{TP}{TP + FN} \% \quad (29)$$

$$\text{Positive predictivity (\%)} = \frac{TP}{TP + FP} \% \quad (30)$$

Two graphs will be representing the output of the MHT algorithm. The first graph depicts the output of the applied transforms as well as adaptive thresholds in each window (Figure 2e and 2g). Observing these figures, one can assess the accuracy of the results and the corresponding parameter values. For appropriate values of thresholds, acceptable results would be expected

Table 3. Performance evaluation of several QRS detection algorithms: Application to MITDB.

Detection algorithm	# of annotations	TP	FP	FN	Error (%)	Se (%)	P+ (%)
This study	109428	109215	160	213	0.34	99.80	99.85
Martinez et al. [2004]	109428	109208	153	220	0.34	99.80	99.86
Li et al. [1995]	104182	104070	65	112	0.17	99.89*	99.94*
Hamilton et al. [1986]	109267	108927	248	340	0.54	99.69	99.77
Pan et al. [1985]	109809	109532	507	277	0.71	99.75	99.54
Moody et al. [1982]**	109428	107567	94	1861	1.79	98.30	99.91

*In this case a discrepancy is found between the claimed results and the review paper [Natalia et al., 2008].

** Also called ARISTOTLE software.

Table 4. Performance evaluation of QRS detection algorithms: Application to QTDB.

Detection algorithm	# of annotations	TP	FP	FN	Error (%)	Se (%)	P+ (%)
This study	86892	86819	94	73	0.19	99.92	99.89
Martinez et al. [2004]	86892	86824	107	68	0.20	99.92	99.88
Moody et al. [1982]	86892	84458	459	2434	3.33	97.2	99.46

Table 5. Performance evaluation of QRS detection algorithms: Application to EDB.

Detection algorithm	# of annotations	TP	FP	FN	Error (%)	Se (%)	P+ (%)
This Study	787103	783992	4134	3111	0.92	99.60	99.47
Martinez et al. [2004]	787103	784059	4077	3044	0.90	99.61	99.48
Moody et al. [1982]	787103	748468	10405	38635	6.23	95.09	98.63

Table 6. Performance evaluation of QRS detection algorithms: Application to TWADB.

Detection algorithm	# of annotations	TP	FP	FN	Error (%)	Se (%)	P+ (%)
This Study	11789	11760	24	29	0.45	99.75	99.80

from the method; however, for very low values of thresholds some waves other than the actual R-waves will be improperly detected. Furthermore, for high values of thresholds some QRS complexes will not be detected correctly. In these two cases, the parameter values should be re-adjusted and the algorithm should be applied again to the original signal until acceptable results are obtained. It should also be noticed that the window length can be adjusted as another parameter so that more accurate results are gained from the algorithm. This window length will generally be equal to 550 ~ 700 milli seconds (this value obtained from practical application of the MHT algorithm) for cases of PVC not observed in the original signal. However, if PVCs exist in the original ECG, the parameter value of 500 ~ 550 milli seconds will lead better results. Finally, in the second Figure, the corresponding R-wave in the original signal is represented. The annotation files of the MIT-BIH Arrhythmia Database include information about normal

beats (N), PVCs (V) and changes in the signal quality (~). The results of the MHT algorithm are compared to this information for the purposes of validation and the outcomes including True Positive (TP), False Negative (FN) and False Positive (FP) values are calculated and presented in Table 3. The resulted values for sensitivity and positive prediction are acceptable results in the context of QRS detection, (Natalia et al., 2008).

Characterization of end-systolic and end-diastolic pulses of the arterial

Blood pressure (ABP) waveform using the MHT algorithm (BPMHT)

In this section, in order to generalize the application of the MHT algorithm, it is applied to ABP waveforms of all 18 subjects of the MIT-BIH Polysomnographic Database (<http://www.physionet.org/physiobank/database/slpdb/>)

Table 7. Performance evaluation of MHT algorithm on high-resolution 24-hour Holter database including a vast spectra of heart rates (CHECK#0, CHECK#1).

Holter record	# of beats	# of PVC*	# of PAC**	TP	FP	FN	Error (%)	Se (%)	P+ (%)
PVCDAT 1-5	188531	53	0	52	0	1	1.89	98.11	100
PVCDAT 6-10	174515	148	0	147	1	1	1.35	99.32	99.32
PVCDAT 11-15	179428	312	0	310	2	2	1.28	99.36	99.36
PVCDAT 16-20	189749	1253	0	1247	9	6	1.20	99.52	99.28
PACDAT 1-4	163934	0	323	322	1	1	0.62	99.69	99.69
PACDAT 5-8	157635	0	611	610	1	1	0.33	99.83	99.83
PACDAT 9-12	107891	0	5513	5505	12	8	0.36	99.85	99.78
PAVDAT 1-4	114204	164	22	185	2	1	1.61	99.46	98.93
PAVDAT 5-8	171315	237	52	287	2	2	1.38	99.31	99.31
PAVDAT 9-12	197591	1153	219	1367	9	5	1.02	99.66	99.35
PAVDAT 13-15	108344	1636	788	2419	14	5	0.78	99.79	99.42
Total	1,753,137	4956	7528	12451	53	33	0.69	99.73	99.58

* Premature ventricular contraction ** Premature atrial contraction.

and the corresponding end-systolic and end-diastolic pulses of the ABP waveform are extracted.

The results of the algorithm applied to blood pressure waveforms are shown in Table 8. The mean values of 99.80 and 99.86% are obtained for sensitivity and positive prediction, respectively.

Simulation of PPF algorithm

In this section, a signal with a chirp frequency is embedded into a colored noise. Then, the variance of the sequence of white noise is increased with a specific increment and the estimated signal is extracted. The standard deviation of the difference between the estimated signal and the original signal is represented in Figure 9. As can be seen in Figure 6b, the standard deviation of estimation will increase linearly with an increase in the noise standard deviation. Therefore, it can be inferred that the performance of PPF algorithm changes in a uniform fashion with an increase in noise standard deviation. In other words, for a considerable increase in noise standard deviation, a uniform performance is resulted from the PPF algorithm. In Figures 10 - 12, HR, SBP, DBP and MAP signals averaged for three typical subjects of the MIMIC II Database are illustrated. Fast fluctuations can be observed in these Figures which are significantly due to regulating mechanisms rather than measurement noises. To obtain more accurate results, these fluctuations should be decreased while the signal mean value should not be destroyed by the reduction algorithm. Due to the difficulties in the recognition of the frequency contents of these fluctuations, common digital filters cannot be implemented for this purpose (Rangayyan, 2002). On the other hand, the reference signal should be known so that adaptive filters can be used (Kay, 1979). Therefore, an appropriate mean estimator is needed to weaken the

fluctuations not similar to white noise. An averaged MAP signal with the corresponding PPF resulted smoothed signal for a typical subject is depicted in Figure 13. The magnified part of Figure 13 illustrates the operation of the PPF algorithm in the elimination of MAP fluctuations. Generally speaking, elimination of the MAP and HR fluctuations will lead to higher stability and accuracy of the detection algorithms.

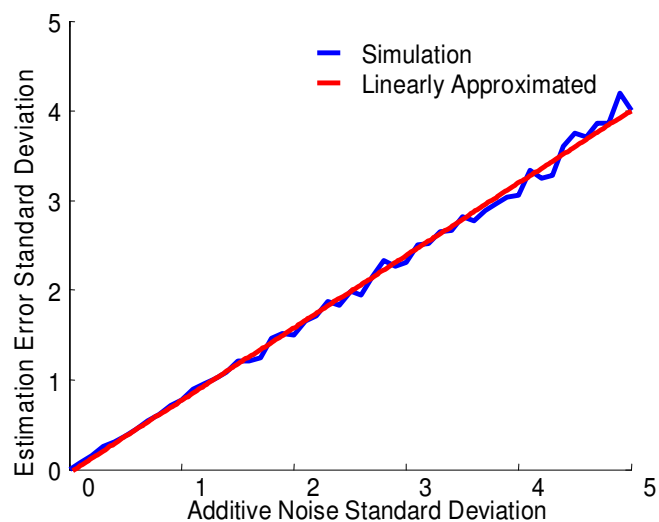
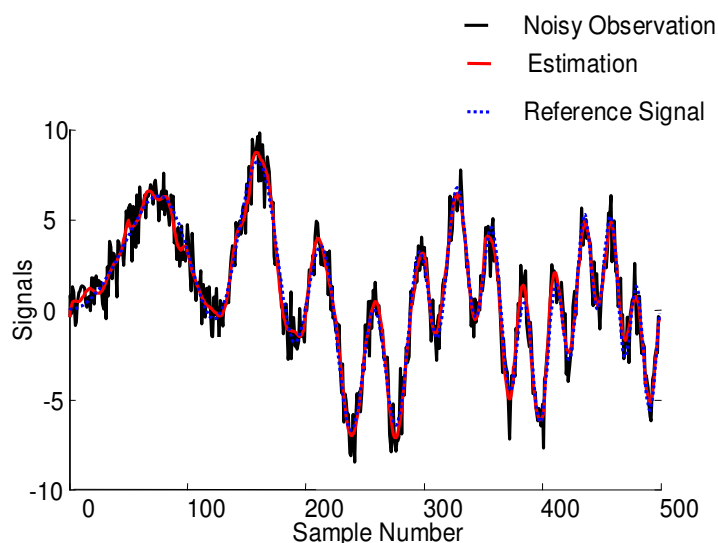
The probability of cardiogenic shock occurrence and scaled MAPDR graphs are represented in Figure 14. The red graphs in this figure have a baseline which is a sign of no MAPDR; however, abrupt increase to the maximum value is an indicator of MAPDR. As can be seen in Figure 14, a high peak between the time 29 and 30 h in the probability of shock occurrence graph is preceded by continuous fluctuations in the corresponding red graph. The results of this study show that all high peaks with 3 to 4 min duration in the probability of shock occurrence graph are preceded by peaks in MAPDR signal with the duration of 20 min or more (Figures 10, 11 and 12). Therefore, as a result of this study, MAPDRs can be used as specific markers for the prediction of cardiogenic shock. It should be noted that there may exist some continuous fluctuations in MAPDR with no corresponding high peaks in the probability of shock occurrence graph. This can be due to short duration of such fluctuations. In summary, these fluctuations should have duration of 20 min or more so that high peaks with the duration of 3 or more minutes occur in probability of shock occurrence diagram.

Conclusion

In this study, in order to consider the mutual influence of parameters on the evaluation of shock probability, a Sugeno Adaptive Network-based Fuzzy Inference System-ANFIS was trained using Hasdai et al

Table 8. Application of the MHT algorithm to the MIT-BIH Polysomnographic Database and obtained results. A total number of 650000 samples is chosen for each record.

MIT-BIH record	Total # of beats	FP	FN	FP+FN	FP+FN (%)	Se (%)	P+ (%)
slp01a	2797	0	5	5	0.18	99.82	100
slp01b	2834	2	3	5	0.18	99.89	99.93
slp02a	4028	0	15	15	0.37	99.63	100
slp02b	3408	0	7	7	0.21	99.79	100
slp03	3158	0	0	0	0	100	100
slp04	3593	0	0	0	0	100	100
slp14	2857	0	0	0	0	100	100
slp16	3768	0	0	0	0	100	100
slp32	3041	0	1	1	0.03	99.97	100
slp37	3620	0	0	0	0	100	100
slp41	2831	50	30	80	1.06	99.4	99.54
slp45	3370	7	7	14	0.42	99.79	99.79
slp48	2981	11	2	13	0.44	99.93	99.63
slp59	3319	0	5	5	0.15	99.85	100
slp60	3271	7	0	7	0.21	100	99.79
slp61	3177	25	7	32	1.01	99.78	99.22
slp66	3093	50	60	110	0.82	99.67	99.51
slp67x	3095	0	36	36	1.16	98.84	100
Total # of subjects		18			Sensitivity %	99.80	
Total # of complexes		58241			Positive predictivity %	99.86	



(a)

(b)

Figure 9(a). Graphical representation of the performance of PPF algorithm: Solid lines are noisy observation as well as signal estimation and dashed line represents the reference signal. **(b)** The standard deviation of estimation error versus standard deviation of the i.i.d. noise sequence

parameters as input, with appropriate membership functions for each parameter. Using this network, it would be possible to incorporate the possible mutual influences between risk parameters such as heart rate (HR), systolic blood pressure (SBP), diastolic blood pressure (DBP), age, gender, weight and some miscellaneous factors to the calculation of shock occurrence probability.

MHT algorithm was introduced for the detection of QRS complexes and blood pressure pulses on the basis of some mathematical operations on the Hilbert transform of the ECGMHT and ABP signals. It was then customized with two versions of ECGMHT and BPMHT to be applied to ECG signal and ABP waveform, respectively. After applying this algorithm to the MIT-BIH Database, the value

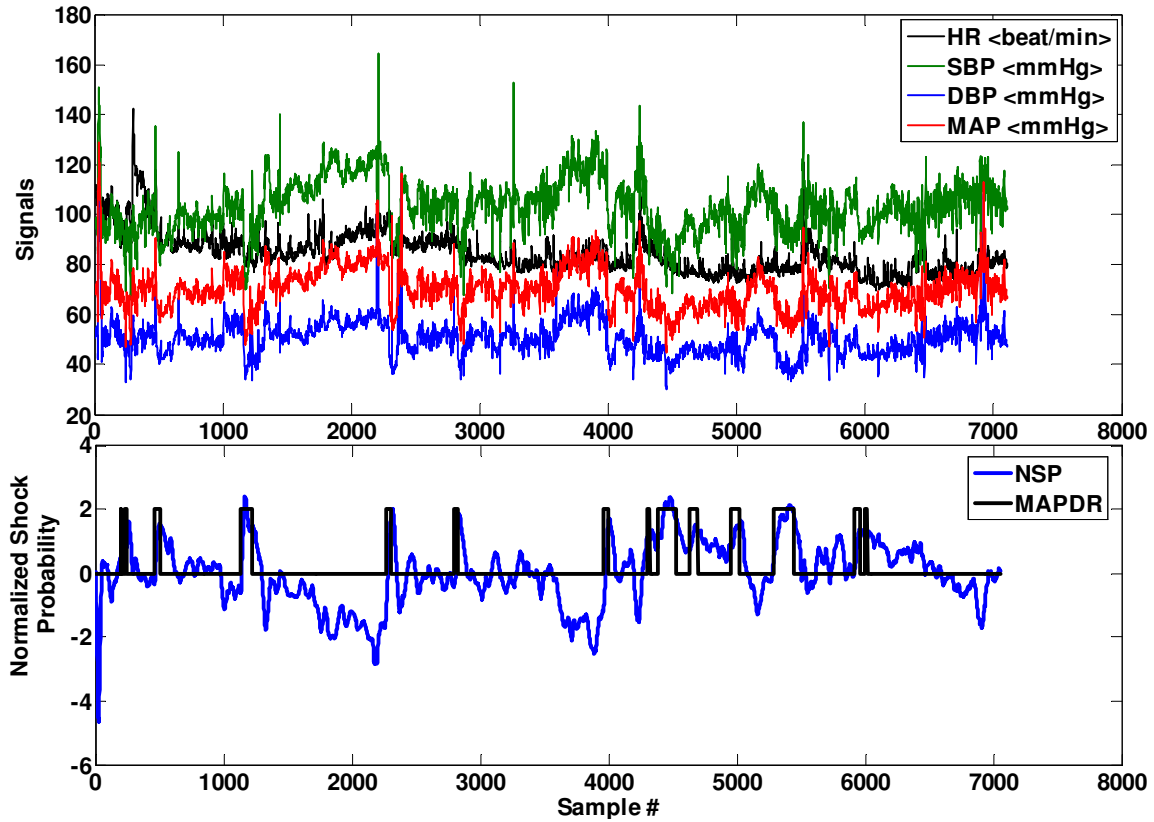


Figure 10. (Top) HR, SBP, DBP and MAP trends averaged in one-minute intervals of s22466 of MIMIC II database obtained as outputs of BPMHT and ECGMHT algorithms, (bottom) normalized shock probability obtained from ANFIS and MAPDR signal.

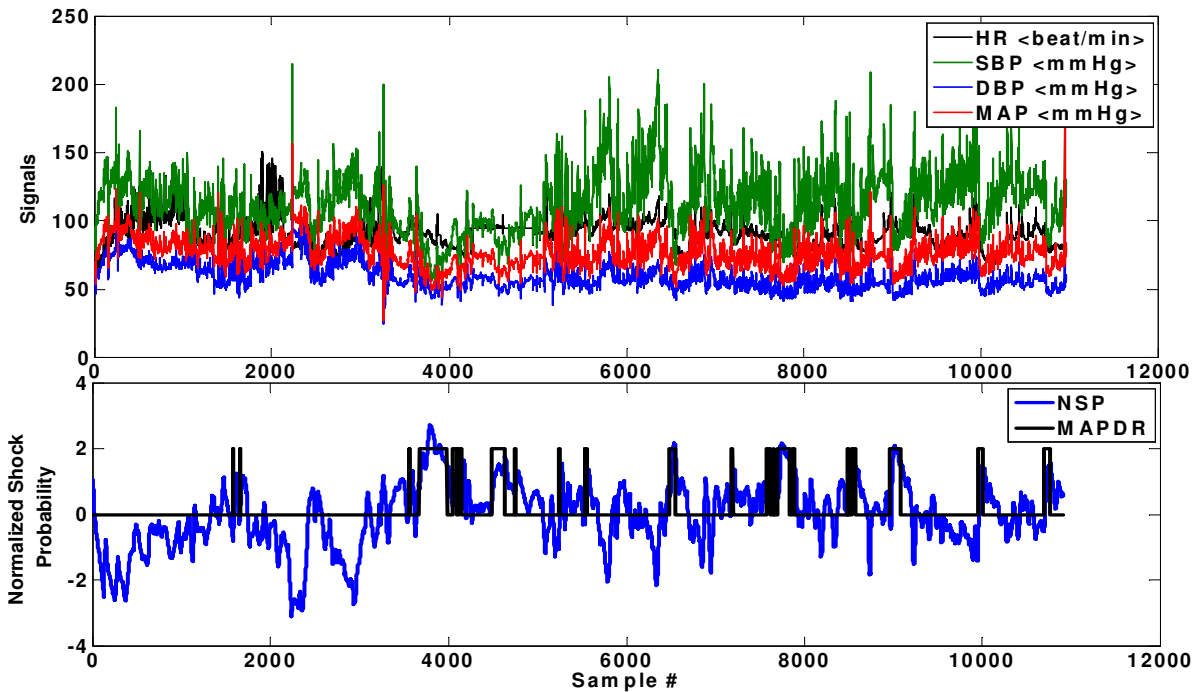


Figure 11. (top) HR, SBP, DBP and MAP trends averaged in one-minute intervals of s24799 of MIMIC II database obtained as outputs of BPMHT and ECGMHT algorithms, (bottom) normalized shock probability obtained from ANFIS and MAPDR signal.

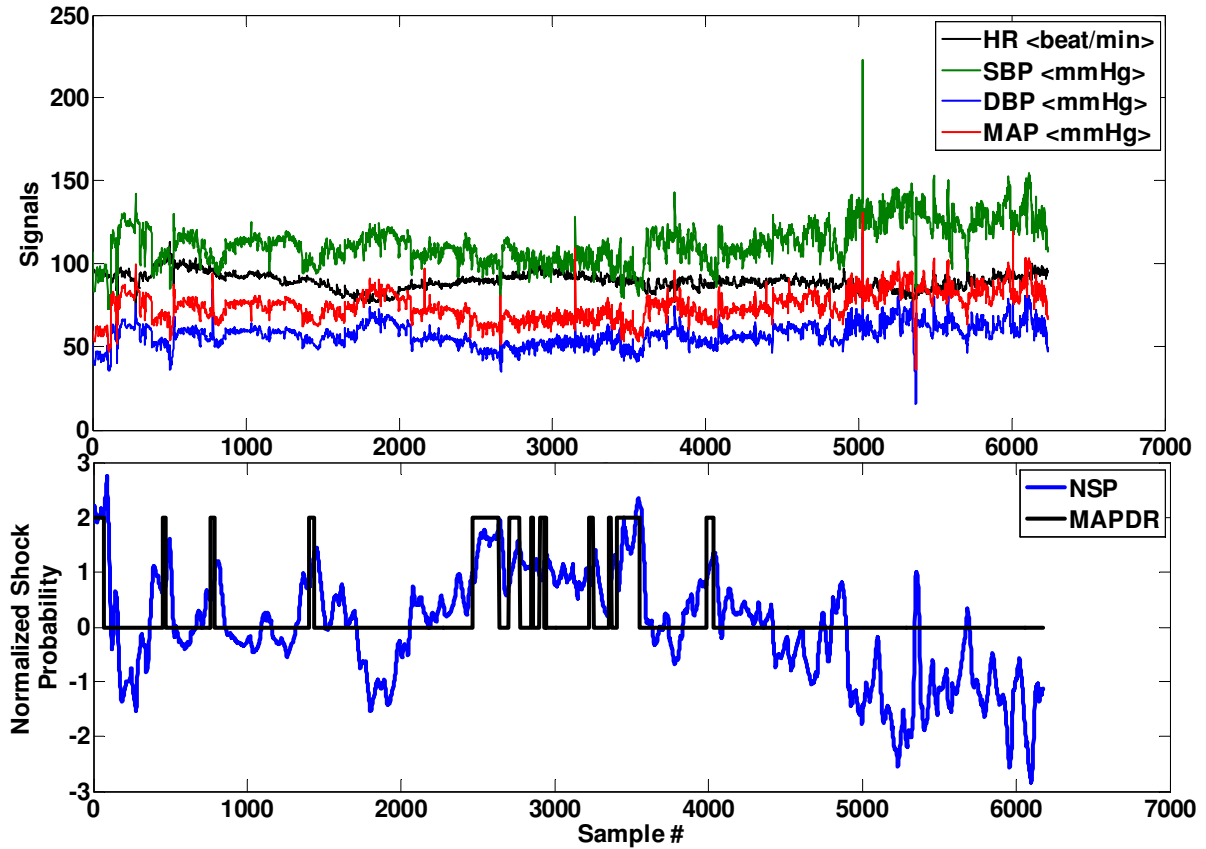


Figure 12. (Top) HR, SBP, DBP and MAP trends averaged in one-minute intervals of s25699 of MIMIC II database obtained as outputs of BPMHT and ECGMHT algorithms, (bottom) normalized shock probability obtained from ANFIS and MAPDR signal.

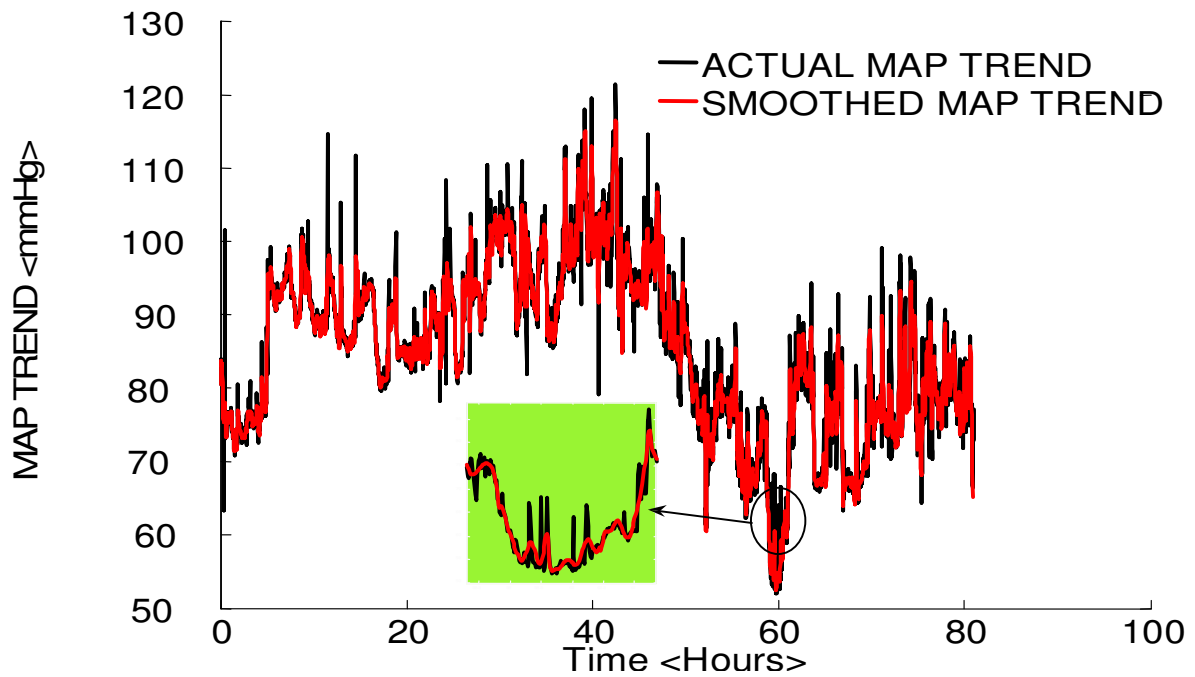


Figure 13. Averaged MAP trend and the corresponding PPF smoothed version for a typical subject. The magnified part shows the capability of the algorithm in the elimination of fast fluctuations

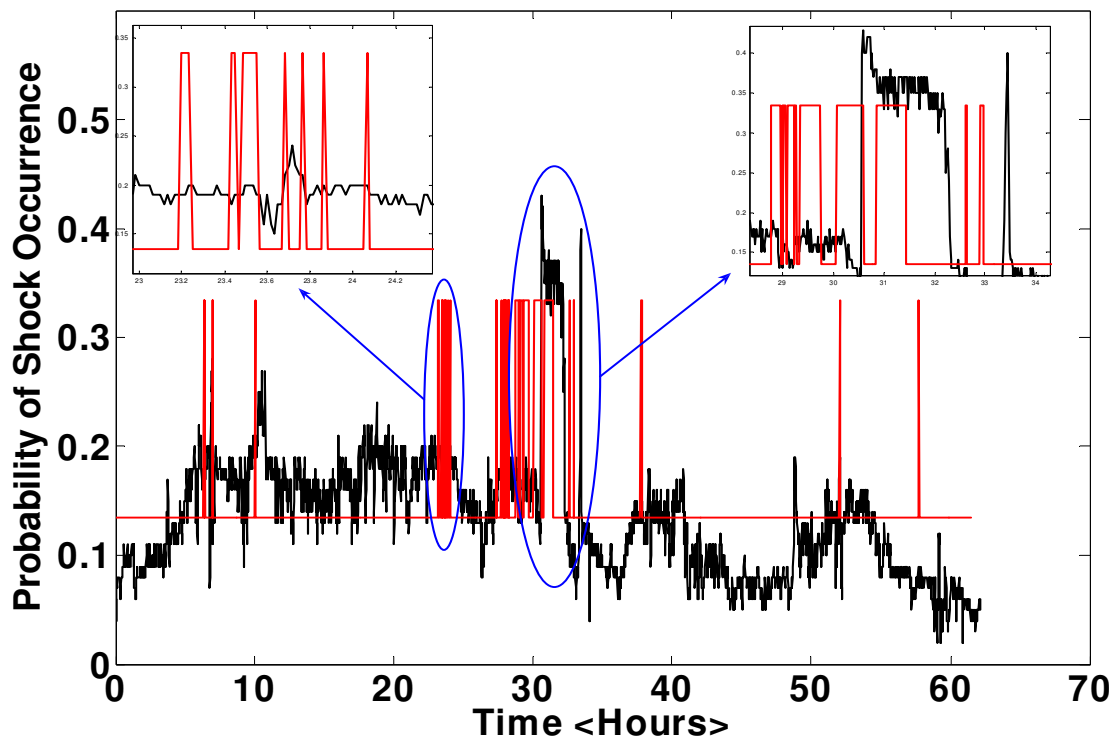


Figure 14. Magnifications in the MAPDR occurrence and cardiogenic shock probability trends. In the left graph, fast fluctuations occur with no high duration. However, fast fluctuations with high endurance as well as a peak in the probability occurrence trend is observed in the right hand plot.

of 99.80 and 99.85% were obtained for sensitivity and positive prediction, which are remarkably acceptable in the field of wave detection.

In the next step, the PPF algorithm was developed for the elimination of fast fluctuations with unknown statistical specifications. The ECGMHT and BPMHT algorithms were then applied to 15 subjects of MIMIC II Database and the resulted averaged MAP, SBP, DBP and HR trends were next smoothed using the FFT algorithm. Afterwards, a new measure entitled as MAPDR was proposed as an indicator of descending behavior in the MAP trend when AHE occurs and was calculated using the resulted PPF signals.

In the next step, using the trained ANFIS model, the probability of shock occurrence for each subject was computed and then depicted. A comparison between the probability of shock occurrence and MAPDR trends indicates that for a sequence of MAPDRs as long as 20 min or more in the MAP trend, there would exist a high peak with the duration of 3 to 4 min in the probability of shock occurrence diagram. Finally, as a result of this study, MAPDRs were specified as appropriate markers of the risk of cardiogenic shock when AHE occurs.

List of acronyms: AHE, Acute hypotensive episode; MHT, modified Hilbert transform; ABP, Arterial blood pressure; SBP, systolic blood pressure; DBP, diastolic blood pressure; MAP, mean arterial pressure;

PPF, piecewise polynomial fitting; BLUE, the best linear unbiased estimation; ANFIS, adaptive network-based fuzzy inference system; MF, membership function; MAPDR, mean arterial pressure dropping regime; HR, heart rate; MIMIC, name of Physionet database; BP, blood pressure; BPMHT, name of the blood pressure pulse detector; ECGMHT, name of the QRS detector; NSP, normalized shock probability; MI, myocardial infarction; PVC, premature ventricular contraction; PAC, premature atrial contraction; FP, false positive; FN, false negative; TP, true positive; Se, sensitivity; P+, positive predictivity; DI, dropping index.

REFERENCES

- Ali G, Mohammad RH (2008). Fading Parameters of Sodium, Potassium and Leakage Ionic Channels the Best Linear Unbiased Sequentially Estimation (BLUE) Via Voltage Clamp Technique Noisy Measurement", 16th Annual (International) Conference on Mechanical Engineering-ISME, Shahid Bahonar University of Kerman, Iran, May 14-16.
- Allen WC, Jean FL, Arthur CG (1973). Role of the Baroreceptor Reflex in Daily Control of Arterial Blood Pressure and Other Variables in Dogs, *Circ. Res.* 32: 564-576.
- Amir H, Mandeep S, Eugenia N, Cindy LG, James ET, Eulogio G, David AC, Mark T, Thomas DS, Yingo N, Alexandra JL, Bernard JG, William WO, Roxana M, Gregg WS (2005). Prediction of Mortality After Primary Percutaneous Coronary Intervention for Acute Myocardial Infarction, The CADILLAC Risk Score", *J. Am. Coll. Cardiol.* 45: 1397-1405.
- Benitez D, Gaydecki PA, Zaidi A, Fitzpatrick AP (2001). The use of the Hilbert transform in ECG signal analysis", *Comput. Biol. Med.* 31: 399-406.
- David H, Robert MC, Trevor DT, Judith SHE, Magnus O, Matthias P, Eric RB Alec V, Paul W, Douglas AC, Eric JT, David R (2000).

- Predictors of Cardiogenic Shock After Thrombolytic Therapy for Acute Myocardial Infarction", *J. Am. Coll. Cardiol.* 35: 136-143.
- Guyton AC (1996). *Text book of physiology*, Philadelphia: W.B. Saunders pp. 53-148.
- Hamilton PS, Tompkins W (1986). Quantitative Investigation of QRS Detection Rules using the MIT/BIH Arrhythmia Database," *IEEE Transactions on Biomedical Engineering* 33: 1157-1165.
- Harrison's Principles of Internal Medicine (2007). 17th Edition, the McGraw-Hill Companies pp. 220-240.
- Hasdai DP, Berger B, Battler A, Holmes DR (2008). Cardiogenic Shock, Diagnosis and Treatment," *Humana Press* pp. 18-47.
- Irvin RS, Rippe JM (2003), "Irwin and Rippe's Intensive Care Medicine", Lippincott Williams and Wilkins, Fifth Edition pp. 246-1080.
- Jang JSR (1993). ANFIS: Adaptive-Network-Based Fuzzy Inference System, *IEEE Trans. Systems, Man, Cybernetics* 23(5/6): 665-685.
- Kohler B, Hennig C, Orglmeister R (2002). The Principle of Software QRS Detection", *IEEE Engineering in Biomedicine and Biology* pp. 42-57.
- Li C, Zheng C, Tai C (1995). Detection of ECG Characteristic Points using Wavelet Transforms," *IEEE Transactions on Biomedical Engineering* 42: 21-28.
- Martinez JP, Almeida R, Olmos S, Rocha AP, Laguna P (2004). A Wavelet-Based ECG Delineator: Evaluation on Standard Databases," *IEEE Transactions on Biomedical Engineering* 51(4): 570-581.
- Michael HP, Ravin D, Lynn AS, Lisa AM, Christopher RT, Vladimir D, Richard S, Ken G, Harvey DW, Judith SH (2003). The SHOCK Trial, Echocardiographic Predictors of Survival and Response to Early Revascularization in Cardiogenic Shock, *Circulation* 107: 279-284.
- Min Z, Jian L, Yi MC, Hong Ma, Jian MX, Jian L, Ling Z, Tao G, Ming HH (2007). A Risk-Predictive Score for Cardiogenic Shock after Acute Myocardial Infarction in Chinese Patients", *Clin. Cardiol.* 30: 171-176.
- Moody GB, Mark RG (1982). Development and Evaluation of a 2-Lead ECG Analysis Program," *The Proc. Comput. Cardiol.* pp. 39-44.
- Morris RW, Watterson LM, Westhorpe RN, Webb RK (2005). Crisis Management During Anesthesia: Hypotension", *Qual. Saf. Health Care* 14(11) e1.
- Natalia MA, Zhi-De D, Chi-Sang P (2008). Analysis of First-Derivative Based QRS Detection Algorithms", *IEEE Transactions on Biomedical Engineering* 55(2): 478-484.
- Pan W, Tompkins J (1985). A Real-Time QRS Detection Algorithm," *IEEE Transactions on Biomedical Engineering* 32: 230-236.
- Paul M (1978). *The ICU Book*, Lippincott Williams and Wilkins", Second Edition pp. 43-218.
- Physionet Signal Achieves, <http://www.physionet.org/physiobank/database/mitdb/> and <http://www.physionet.org/physiobank/database/slpdb/>.
- Rangaraj MR (2002). *Biomedical Signal Analysis*", IEEE Press, John Wiley and Sons pp. 40-103.
- Soderstrom T, Stoica P (1989). *System Identification*", Hemel Hempstead, UK: Prentice-Hall International pp. 24-100.
- Solem K, Nilsson A, Sornmo L (2004). Detection of Hypotension during Hemodialysis Using the ECG", *Comput. Cardiol.* 31: 717-720.
- Steven MK (1979). *Fundamentals of Statistical Signal Processing: Estimation Theory*", Prentice- Hall Inc. pp. 40-84.